Effectiveness Of Copper Aluminium Carbonate Layered Double Hydroxide For The Adsorptive Removal Of Anionic Pollutant From Aqueous Solution: Equilibrium, Kinetics, Isotherm

Dhivya R

Head, Assistant Professor

Department of Chemistry

Sri Sarada Niketan College of Science For Women, Karur, India.

Abstract

Environmental pollution caused by the discharge of dye-containing industrial effluents poses a serious threat to aquatic ecosystems and human health. Synthetic dyes, particularly anionic dyes used extensively in textile industries, are highly stable, toxic, and resistant to conventional wastewater treatment methods. In the present study, Copper Aluminium Carbonate Layered Double Hydroxide (Cu/Al-LDH) was synthesized via the co-precipitation method and evaluated as an efficient adsorbent for the removal of Acid Violet dye from aqueous solution. The adsorption performance of Cu/Al-LDH was systematically investigated through equilibrium, kinetic, isotherm, and thermodynamic studies. The results demonstrated that Cu/Al-LDH exhibits high adsorption capacity toward Acid Violet due to its layered structure, large surface area, and strong anion-exchange ability. The adsorption process was found to be favorable and spontaneous, indicating effective interaction between the anionic dye molecules and the LDH surface. The study confirms that Cu/Al-LDH is a low-cost, environmentally benign, and promising alternative adsorbent for the treatment of dye-contaminated wastewater.

Key words: Copper–Aluminium LDH, Acid Violet dye, Adsorption, Isotherm studies, Wastewater treatment

I. INTRODUCTION

Environmental Pollution is of paramount concern that challenges the human life through Increase in water pollution causing adverse impacts upon availability of fresh water. Though 70 Percent of World is covered by Water, only around 3% of it remain as Fresh water. The rapid increase in toxic dye wastewater generated from various industries remains a severe public health issue and posing a major challenge to existing conventional water treatment systems. The release of colored effluent into recipient streams diminishes the aesthetic value of water and limits the penetration of sunlight into the water, hence diminishing its photosynthetic capabilities. The Proportion of industrial wastewater flow treated was 30% and Globally, 56% of household wastewater flows were safely treated. Colorants such as dyes are among the harmful substances discharged into the aquatic environment by various industrial activities, including the Dye Manufacturing, Paper, Leather, Tanning, Textile, Printing, Coloring cellulosic fibers, and Creating related combinations.

Textile Industries among those that use 6x10 tonnes per year and approximately 15% of dyes released into water. The presence of dyes and pigments substantially have negative impacts on aquatic fauna and fauna. Among the synthetic dyes used in textile industries Azo Dyes plays a prominent role that accounts for 60% of the total. Dyes are anionic, water-soluble, and contain functional groups that react with a wide range of substances via the formation of covalent bonds, ion-exchange effect, and complexation effect. Dye is a compound which consists of both Chromophore and Auxochrome, Chromophore impart colour to the substance whereas Auxochrome increase the intensity of that colouring substance. Traditional waste water treatment technologies have been proven to be markedly ineffective for handling waste water of synthetic textile dyes because of the chemical stability and toxicity. Therefore, the treatment of industrial dye effluents requires practical and cost-effective methods. The effluent discharge of the textile industry leads to environmental pollution owing to the existence of complex mixtures of methylene green (MG), methyl orange (MO), and malachite blue (MB) as cationic and anionic dyes and toxic metal ions in polluted water. Thus, different chemical and physical techniques have been applied, such as biodegradation, reverse osmosis, activated sludge, chemical oxidation, and electrochemical methods involving membrane separation, chemical oxidation, anaerobic and aerobic microbial degradation, Adsorption, and Photo degradation.

Adsorption is the process of transference of mass where one or more Adsorbate present in gaseous or liquid stream is transferred in a selective way to the surface of a porous solid (Adsorbent), It has been emerged as simple and environmental benign processes for wastewater treatment. It has been selected as a potential technique to treat wastewater due to its scalable synthesis of adsorbents, high removal efficiency and cost effectiveness. Many materials have been used as Adsorbents including Activated Carbon, Zeolites, Oxides, Graphene Oxides, Composites, Polymers, Carbon Nanotubes. Though Activated carbon, which is widely used as an adsorbent for wastewater treatment, it is expensive and therefore, uneconomical. Many investigators have been studied the feasibility of using inexpensive alternative materials like Pearl millet husk, Date pits, Saw dust, Buffing dust of leather industry, Coir pith, Crude oil residue, Tropical grass, Olive stone, Almond shells, Pine bark, Wool waste, Coconut shell etc., as carbonaceous precursors for the removal of dyes from water and wastewater. Thus the removal of organic pollutants with the use of Layered Double Hydroxide(LDH) has been of great interest to many researchers in recent years, This is because of its unique features and properties, such as high surface area, low toxicity, low cost, high capacity of anion substitution, recoverability and high stabilities for chemical and thermal properties. Several techniques have been reported for the modification of LDHs.

Layered Double Hydroxides are class of layered materials with General Formula of $[(M^{2}).\ (M^{3})(OH):]+(A-x/m).nH_2O$, where M, Mand A represent Divalent Metal cations, Trivalent Metal cations and an Interlayer anion, x was denoted as the Molar ratio of M^{3} to total metal, ranging from 0.2 to 0.33 for pure LDH formation. As an Anionic clay, LDH based materials in the area of Adsorption of a variety of dyes onto L.DHs with different M cations has been reported recently. Co-precipitation is usually used for the preparation of pure LDH, in which solution containing metals is mixed with a basic solution (such as NaOH solution) and the LDH solid is obtained via separation and drying. In the present study, Copper Aluminium Carbonate LDH (CuAI-LDH) material is prepared and used for the removal of Acid Violet from aqueous solution. The adsorption equilibrium and thermodynamic studies for the adsorption of Acid Violet onto the prepared material of Cu/AIC-LDH material has been investigated. The main aim of the present work is to study the suitability of the prepared Cu/AI-LDH for the removal of Acid Violet from aqueous solution by adsorption method.

II. AIM AND OBJECTIVE OF THE STUDY

Since synthetic dyes are toxic and carcinogenic in nature, it is considered as an objectionable type of pollutant. Even a trace amount of dyes in aqueous medium is highly visible and interfere the transmission of light and upset the biological metabolism in aquatic ecosystem. In order to solve the problem in the environment, a wide range of physical and chemical methods have been developed for the removal of synthetic dyes from waters and wastewaters. The adsorption process is one of the effective methods used to remove dyes from aqueous solution. Activated carbon is the most widely used adsorbent for dye removal, but it is too expensive. Marry investigators have studied the feasibility of using inexpensive alternative materials like pearl millet husk, date pits, saw dust huffing dust of leather industry, coir pith, crude oil residue tropical grass, olive stone and almond shells, pine hark, wool waste, coconut shell etc., as carbonaceous precursors for the removal of dyes from water and wastewater. In this present study, Copper Aluminium Carbonate Layered Double Hydroxide (Cu/Al-LDH)) was synthesized and used for the adsorption of Acid Violet (AV) dye from aqueous solution. The equilibriom and thermodynamic studies for the adsorption of AV onto the Cu/Al-LDII has been investigated and the results are discussed in the following pages

III. MATERIAL AND METHODS

3.1 MATERIALS

3.1.1 PREPARATION OF Cu/Al-LDH

All of the materials utilized in this investigation are AR grade and have not been purified in any way. The Copper Aluminum Layered Double Hydroxide (Cu/Al-LDH) is synthesized using a co-precipitation technique in a 500ml reaction flask with an aqueous solution of CuSO4.6H_2O and Al(SO) 16H_2O in a molar ratio of M^2/M^3 2:1. Add a solution of freshly made sodium hydroxide (1M) (precipitating agent) and sodium carbonate (1M) (intercalating carbonate anion source) drop wise until the pH reaches 10. The resulting slurry is continually agitated to about 6 hours in a magnetic stirrer. The material is next filtered and rinsed multiple times with distilled water until the pH is neutral, then dried in a hot air oven at 80 degrees Celsius. The produced material are kept in a vial and used for future studies.

3.2 METHODS

The prepared Cu/Al- LDH were finely powdered and characterized by P-XRD, FTIR, SEM with EDX.

3.2.1 CHARACTERIZATION OF Cu/AI-LDH

The prepared Mg/AL-LDH sample was crushed in to fine finely powdered and characterized by P-XRD, FTIR, SEM with EDS analysis.

3.2.1.1 Scanning Electron Microscope with Energy Dispersive Spectroscopy

Further the surface morphology and elemental composition of samples are analyzed by using Field Emission Scanning Electron Microscope (FESEM-ZEISS SIGMA GEMINI) with Energy dispersive spectroscopy (EDS), Samples were coated with a gold/palladium film, and the FESEM images were obtained using a secondary electron detector.

3.2.1.2 Fourier Transform Infrared Spectroscopy

The functional groups of the as-prepared samples were observed by the Fourier Transform Infra-Red spectroscopy (FTIR-Perkin Elmer, USA) using a KBr pellet over the range of 4000-400cm^{-1}.

3.2.2. PREPARATION OF SYNTHETIC DVE SOLUTION

The dye used for the adsorption study is Acid Violet (AV). The molecular formula is $C_{41}H_{48}N_3NaO_6S_2$, with Colour Index: 42650 and molecular weight: 765.96. The concentration of AV in each aqueous solution was measured on an UV-Vis Spectrophotometer 117 at λ_{max} = 548nm. The molecular structure of the dye is shown in Figure 1.

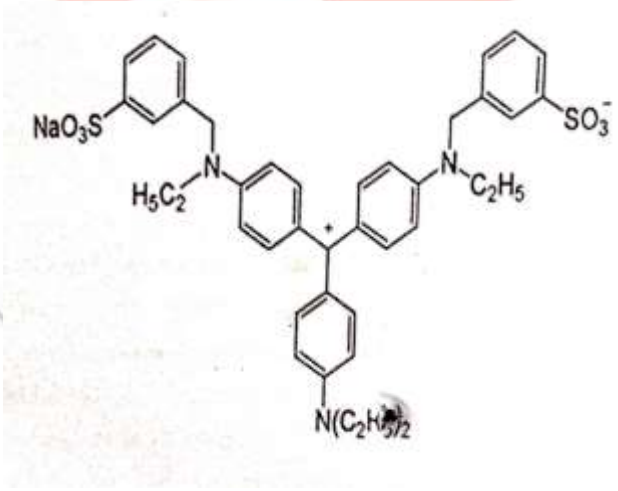

Figure 1. Molecular Structure of Acid Violet

The experimental dye stock solution was prepared by dissolving exactly Ig of Acid Violet (AV) in 1000 ml of double distilled water. Further, the dye solutions of the relevant concentrations (10 - 100 mg/L) were obtained by serial dilutions from the stock solution. All of the chemicals used were analytical reagent grade and distilled water was used throughout the investigation.

3.2.3 ADSORPTION STUDIES

3.2.3.1 Batch Adsorption Studies

Adsorption of 10 mgI^{-1} was determined at different wavelengths using UV visible spectrophotometer to obtain a plot of absorbance verses wavelength. The wavelength corresponding to the maximum absorbance (λ_{max} = 548 nm) as determined from the plot was noted. This wavelength was used for measuring the absorbance of residual concentration of Acid Violet (AV) dye. The efficiency of an adsorbent was evaluated by conducting batch mode experiments. The experiment was carried out by using 50 mg adsorbent with 100ml of dye solution varies from 10 mgl $^{-1}$ to 100 mgl $^{-1}$ concentration at 150 rpm speed on an REMI made orbital shaker. The mixture was withdrawn at specified intervals and filtered. The unadsorbed supernatant liquid was analyzed for the residual dye concentration using Colorimeter at the wavelength 548 nm. The pH of the solution was adjusted using IM HCl and IM NaOH. pH meter was used to adjust the pH of dye solution as per the requirement. The effect temperature was also studied for 30ºC, 40ºC and 50ºC. All experiments were carried out in duplicate for accuracy.

3.2.3.2 Adsorption Kinetics Studies

The prediction of the adsorption kinetics of dye from aqueous system is very important to design a suitable treatment system. In order to analyze the adsorption kinetics of Acid Violet (AV) dye onto Cu/Al-LDH, the following kinetics models have been studied.

Pseudo-First Order Kinetics

The first order equation is the simplest one and is the most widely used for the adsorption of a solute from a liquid solution. The equation is given below

$$dq/dt = k_1(q_e - q_t) \quad \text{-------} \quad (1)$$

which was further integrated to

$$\log(q_e - q_t) = \log q_e - (k_1 / 2.303)_t \quad \text{-------} \quad (2)$$

where, q_e and q_t are the amounts of dye adsorbed at equilibrium and time t (min), k_1 is the rate constant (min^{-1}). Linear plot of $\log(q_e - q_t)$ versus t gives the value of $k_1$and qe.

Pseudo-second order model

The pseudo-second order kinetic model has been used to describe the adsorption mechanism by the adsorbents when the adsorption process does not follow the pseudo-first order kinetics. In addition it provides the information about the rate limiting step of adsorption mechanisms by either physical or chemical sorption process.

$$(dq/dt) = k_2(q_e - q_t)_2 \quad \text{---------} \quad (3)$$

On integration of equation 3 for the boundary conditions t = 0 to t = t and q = 0 to q = q_t, the equation can be expressed as

$$1/(q_e - q_t) = 1/ q_e + k_2 t \quad \text{---------} \quad (4)$$

The equation 4 can be rearranged to linear form is given as

$$(t/ q_t) = 1 / k_2 q_e^2 + (1/q_e)\, t \quad \text{------} \quad (5)$$

where, k_2 is the second order rate constant (g/mg min) and q_e is the equilibrium adsorption capacity (mg / g). A graph is plotted between t/ q_t versus t for different initial concentrations and temperature. If the graph obtained is linear form, the adsorption process follows second order kinetics. The value of qe and k_2 can be calculated from the slope and the intercept of the plot.

3.2.3.4 Adsorption Isotherm

Adsorption isotherms are generally used for the design of adsorption system. The Langmuir and Freundlich equations are commonly used for describing the adsorption isotherms. The linear equations of Langmuir and Freundlich are represented in the following equations (6) and (7) respectively.

$$C_e / Q_e = (C_e / Q_e) + (1 / Q_0 b) \quad \text{------} \quad (6)$$

$$\text{Log } Q_e = 1 / n \log C_e + \log K_f \text{ ------ (7)}$$

were C_e and Q_e were amount of dye adsorbed at equilibrium (mg/g), equilibrium concentration (mg / g) and Qo and b are the Langmuir constants, indicating the adsorption capacity and energy of adsorption respectively. K_f and n are the empirical constants of the Freundlich isotherm measuring the adsorption capacity and intensity of adsorption respectively.

3.2.3.5. Thermodynamic Parameters

The standard free energy change (ΔG^o) , enthalpy change (ΔH^o) and entropy change (ΔS^o) were calculated from the variation of the thermodynamic equilibrium constant K. The K for the adsorption process and the thermodynamic parameters were calculated using the following equations,

$$K = C \text{ Solid} / C \text{ liquid -------- (8)}$$

$$\ln K = (\Delta S^o / R) - (\Delta H^o / RT) \text{ ------ (9)}$$

$$\Delta G^o = - RT \ln K \text{ ------- (10)}$$

ΔH^o and ΔS^o were determined from the slop and intercept of the plot of ln K versus 1/T respectively.

IV. RESULTS AND DISCUSSION

4.1 SURFACE AND FUNCTIONAL CHARACTERIZATION OF Cu/Al-LDH BY XRD, SEM, EDS and FTIR 4.1.1 XRD Analysis of Cu/Al LDH

The XRD patterns of synthesized Copper Aluminium Carbonate LDH (Cu/AI-LDH) fitted well to the characteristic reflections of regular layered structure of LDH materials. The basal reflections of planes hkl (003), (006), (012), (015), (110) & (113) were also resembled with previous study. High crystallinity of the synthesized material was supported by the increased intensity and the sharpness of the peak at lower 20 value from XRD pattern. Furthermore, an Intense reflection attributed to a secondary phase and Al(OH); was seen around the higher 20 value in the range of 35°-60°.

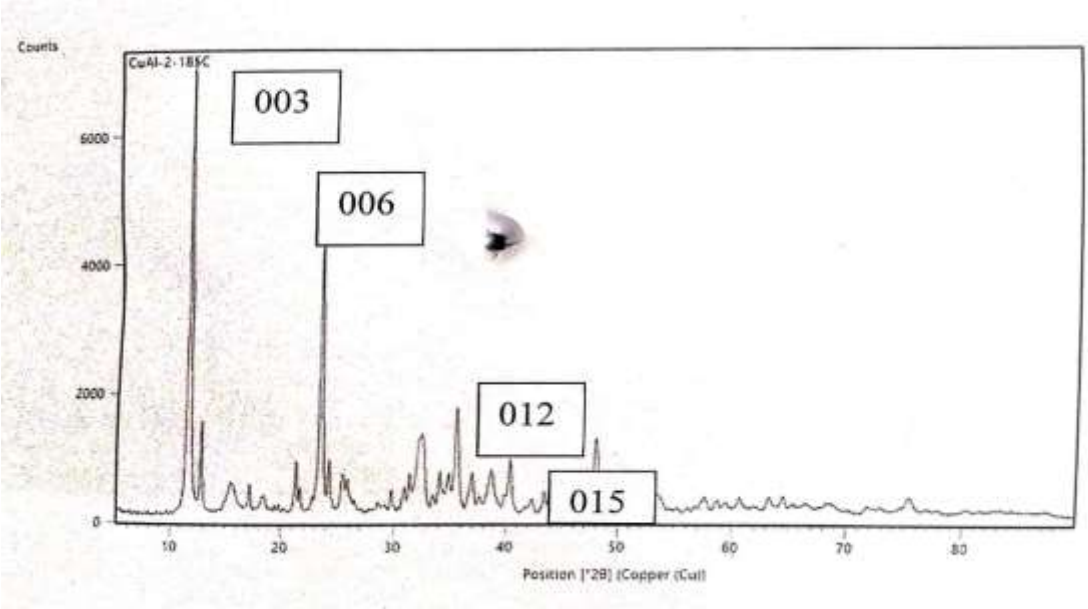

Figure 2 XRD Pattern of Cu/Al LDH4.1.2 SEM and EDS Analysis of Cu/Al LDH before and After Adsorption of AV dye

The SEM images of both the material Cu/Al-LDH before and after adsorption of the select Jye of Acid Violet (AV) are shown in Figures 3 (a) & (b). The SEM image of the synthesised LDH materials shows that they are rectangular plate like structure with porosity. The adsorption of Acid Violet (AV) dye on to Cu/Al-LDH was evidenced that the adsorbate molecule was well bounded well to the surface of the adsorbent material Cu/Al-LDH and was shown in Figure 3(b).

Figure 3. SEM image of Cu/Al-LDH (a) before adsorption (b) after adsorption of Acid Violet (AV)

The Presence of elements and its ratio in the synthesized materials were determined by EDS and are shown in Figure 4 (a) and (b). The calculated final ratio of (Cu^{2+}/Al^{3+} = 2) obtained from the analysis was close to the initial ratio (as prepared in the mother liquor). The other elements like Hand C in the form of Hydrate and carbonate were present in the sample confirmed by the FTIR.

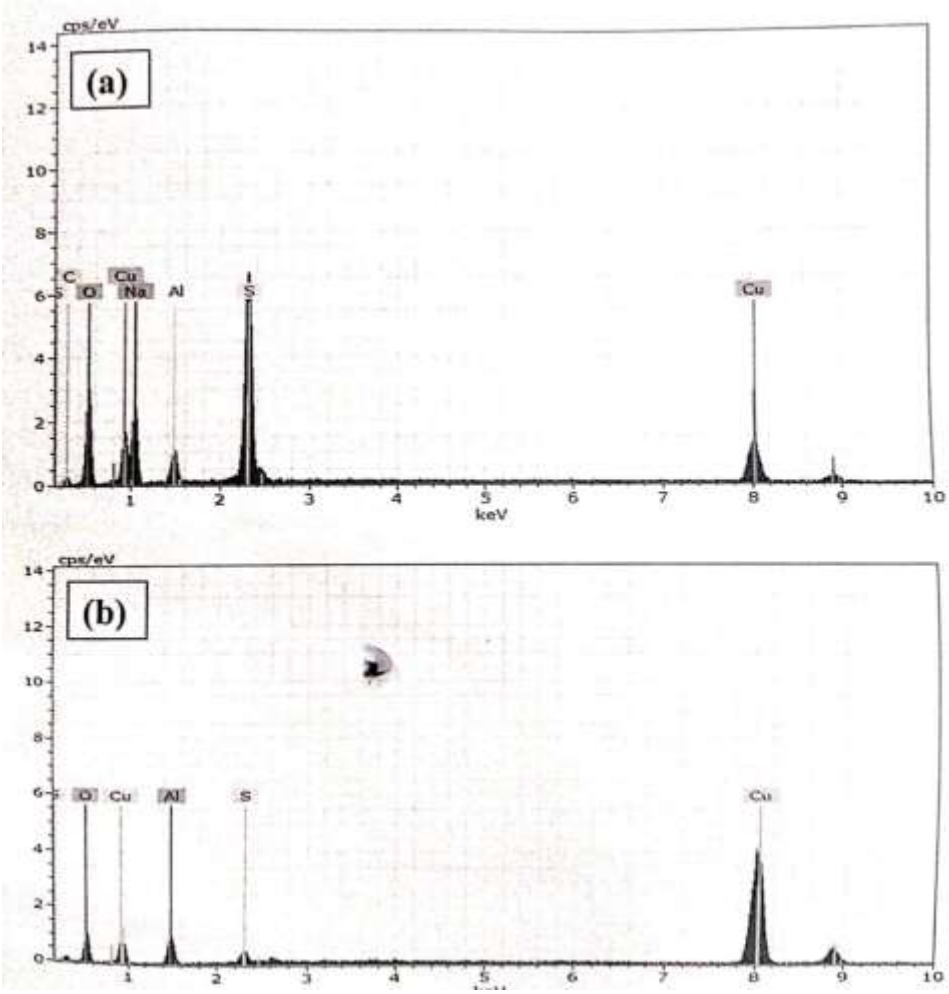

Figure 4. Energy Dispersive Spectrum of Cu/Al-LDH (a) before Adsorption (b) After Adsorption of Acid Violet

4.1.3 FTIR Spectrum Analysis of Cu/Al LDH before and After Adsorption of AV

Fourier transform infrared spectra (FT-IR) were obtained with Perkin Elmer Precisely, Spectrum 100 FT-IR Spectrophotometer in the range of 4000-400 cm^{-1} by the standard KBr pellet technique. FTIR spectra for Cu/Al-LDH before and after adsorption of AV are shown in the Figure 5. The FTIR spectra for Cu/AI-LDH and Cu/AI-LDHAV show a broad absorption band in the 4000-3000 cm^{-1} region centered at around 3205 and 3405 cm^{-1} respectively are due to the presence of O-H stretching mode of the hydroxyl group in the layers, physisorbed and as well as interlayer water molecules. This is commonly observed in the LDHs materials the band at 1370 cm^{-1} is due to H-O-H bending vibration of the interlayer water. The bands in the low frequency region, 400 - 800 cm^{-1} in Cu/Al-LDHAV corresponds to the lattice vibration modes of M-O and O-M-O (M = Cu, Al) . At about 1345 cm^{-1} and 1567 cm^{-1} sharp peaks represents symmetric and asymmetric stretching absorption of C=O group. The appearance of new stretching vibrations at 1187 cm^{-1} supports the sulphonate ($O = S - SO_3^-$) that corresponding to AV dye appear in Figure 5 (b) and decreased intensity of the peak at 1031 cm^{-1} compared with the material at 1093 cm^{-1} before adsorption confirms the adsorption of dye onto the adsorbent material. The aromatic ring present in the dye molecule is confirmed by the appearance of absorption band that appears at 1709 cm^{-1} in Figure 5 (b).

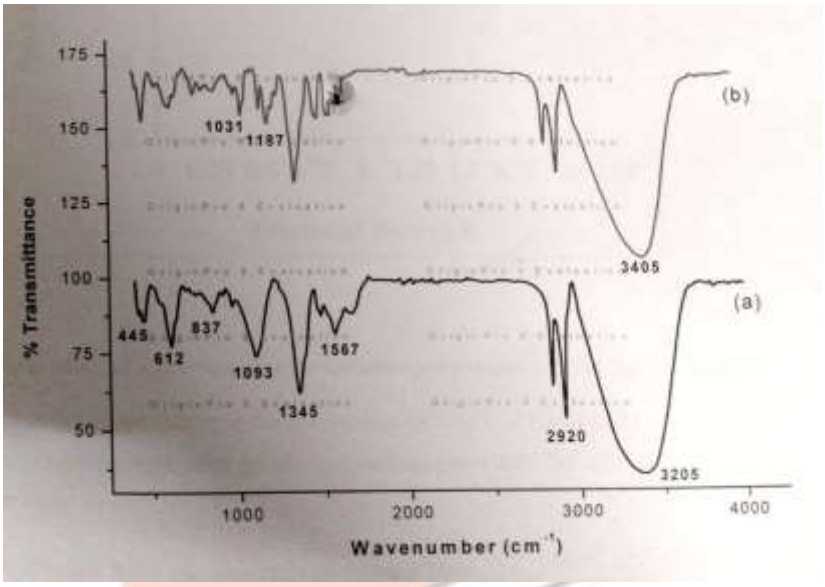

Figure 5. FTIR Spectrum of Cu/Al-LDH (a) before and after adsorption of AV

4.2 Effect of adsorbent dose

The effect of adsorbent dose for the removal of AV onto Cu/AL-LDH is shown in Figures.6. There is an increase in adsorption with the increment of adsorbent dose for 50 mg/L. initial dye concentration and this is attributed by the increased surface area and availability of more adsorption sites. The efficiency of dye removal was 90.00% using 1.0g/L. of Cu/Al-LDH

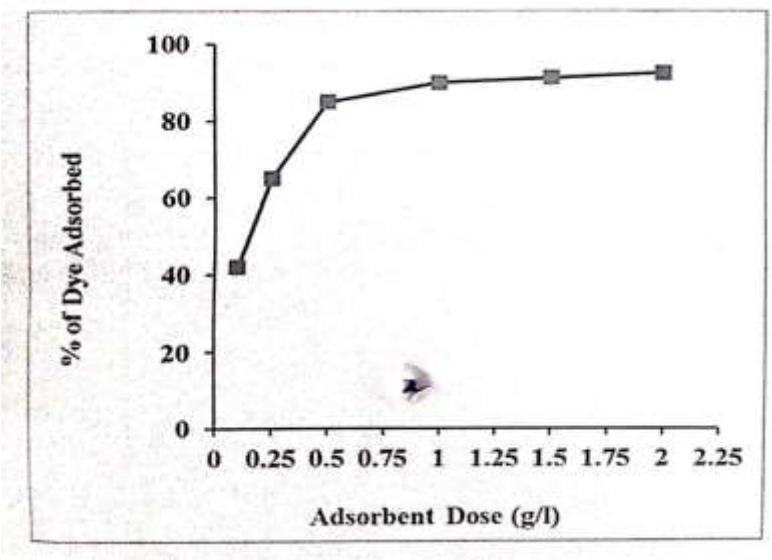

Figure 6. Effect of adsorbent dose for the adsorptive removal of AV by Cu/Al-LDH

There was no significant change in the dye removal after Ig/L of Cu/Al-LDH and it was due to attainment of equilibrium between the adsorbate and adsorbent. The optimized dose was used for further study.

4.3 Effect of Initial Dye Concentration and Contact Time

The experimental results of percentage of adsorption of Acid Violet onto Cu/Al-LDH at various initial concentrations (25, 50, 75 and 100 ppm) with contact time are shown in the Figures 7. The percentage of dye adsorption was decreased from 97.78% to 87.33% while on increasing the initial dye concentration from 25 mg/L to 100 mg/L, but the actual amount of dyes adsorbed per unit mass of LDH material was increased with increase in dye concentration. The amount of AV dye adsorbed was found to increases from 24.44 to 87.33 mg/g by Cu/Al-LDH. This shows that the adsorption is highly dependent on initial concentration of dye. It is because that at lower concentration the ratio of the initial number of dye molecules to the available surface area is low. However, at high concentration the available sites of adsorption become lesser and hence the percentage removal of dye gets decreased with increase in initial concentration.

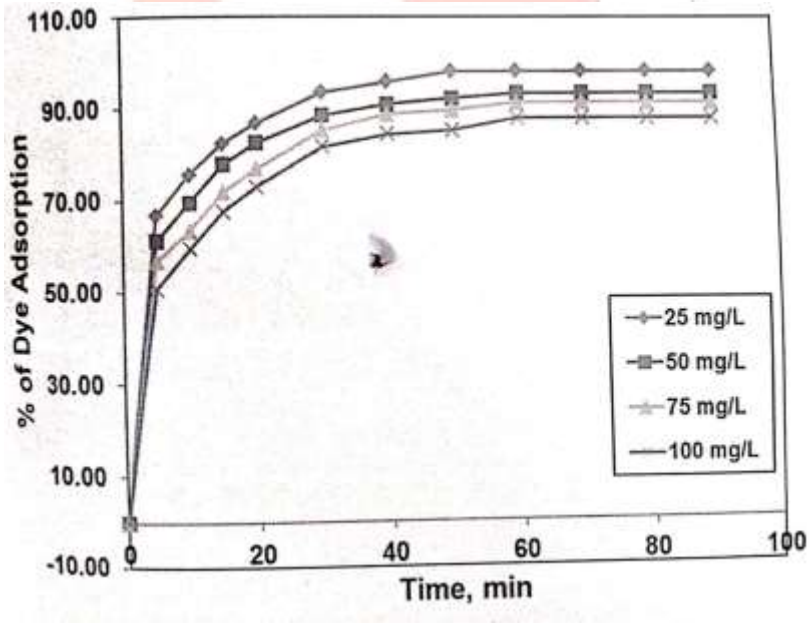

Figure 7. Effect of initial dye concentration on the percentage removal of AV by Cu/Al-LDH

4.4 Effect of pH

The pH is one of the most important factor that controlling the adsorption of dye onto the adsorbent. The effect of pH for the removal of AV by Cu/Al-LDH was performed at different initial solution pH varying between 2 and 12. Figure 8 clearly shows that the maximum dye removal 90% was observed at optimum pH of 3 and almost remains constant upto pH10 by Cu/Al-LDH. This removal was associated with surface charge and availability of bonding sites present on the surface of the Cu/AI-LDH.

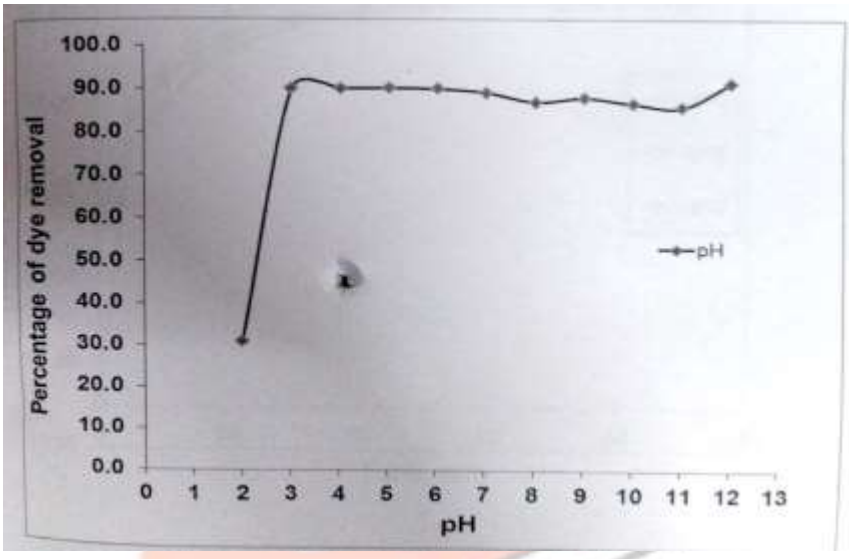

Figure 8. Effect of pH on percentage removal of AV by Cu/Al LDH

4.5 Effect of Temperature

The effect of temperature on the adsorption capacity of the Cu/Al-LDH for the removal of TB dye was studied by varying the temperatures from 30-50°C. The percentage of dye removal was increased with increase of temperature for the materials and is shown in Figure 9. The increase in the equilibrium adsorption capacity of AV dye indicates that a high temperature favours the dye removal. The percentage and the amount of AV removal (Initial dye Concentration 50mg/L) by Cu/Al-LDH was increased from 92.94% to 96.47%. This is shown in the figure 9. From the above results it is clear that adsorption equilibrium is a temperature dependent process and endothermic in nature. This effect may be due to the fact that at higher temperature, an increase in the movement of the solute occurs.

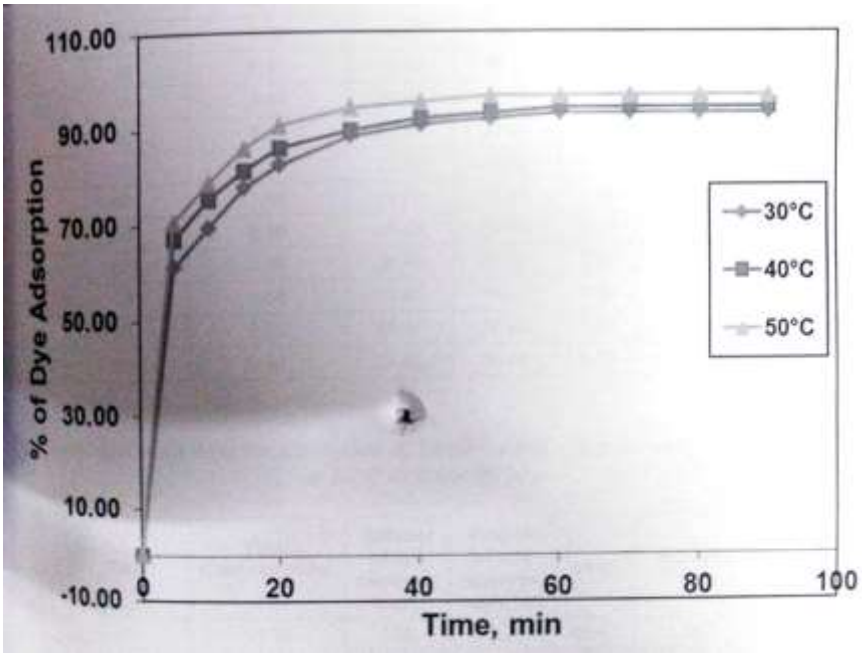

Figure 9. Effect of temperature on the percentage removal of AV by Cu/Al-LDH

4.6 Adsorption Kinetics

The prediction of the adsorption kinetics of dye from aqueous system is very important to design a suitable treatment system. In order to analyze the adsorption kinetics of AV by Cu/Al-LDH, the kinetic studies are carried out for concentration and temperature variations and the data are given in Table 1 to 6.

S.No	Time	Final Concentration, Ce	Amount of dye removed, mg/L	Amount of dye removed, mg/g (qt)	qe-qt	log (qe-qt)	t/qt	ln t	$t^{1/2}$
1	0	25.00	0.00	0.00	24.44	1.388		--	0.00
2	5	8.33	16.67	16.67	7.77	0.891	0.300	1.609	2.23
3	10	6.11	18.89	18.89	5.55	0.744	0.529	2.303	3.16
4	15	4.44	20.56	20.56	3.88	0.589	0.730	2.708	3.87
5	20	3.33	21.67	21.67	2.77	0.443	0.923	2.996	4.47
6	30	1.67	23.33	23.33	1.11	0.044	1.286	3.401	5.47
7	40	1.11	23.89	23.89	0.55	-0.259	1.674	3.689	6.32
8	50	0.56	24.44	24.44	0.00	-	2.045	3.912	7.07
9	60	0.56	24.44	24.44	0.00	-	2.455	4.094	7.74
10	70	0.56	24.44	24.44	0.00	-	2.864	4.248	8.36
11	80	0.56	24.44	24.44	0.00	-	3.273	4.382	8.94
12	90	0.56	24.44	24.44	0.00	-	3.682	4.500	9.48

Table 1. Kinetic data for adsorption of [Acid Violet] =25 ppm onto Cu/Al-LDH at 30 °C to about 90 min

S.No	Time	Final Concentration, Ce	Amount of dye removed, mg/L	Amount of dye removed, mg/g (qt)	qe-qt	log (qe-qt)	t/qt	ln t	$t^{1/2}$
1	0	50.00	0.00	0.00	46.47	1.667	-	--	0.00
2	5	19.41	30.59	30.59	15.88	1.201	0.163	1.609	2.23
3	10	15.29	34.71	34.71	11.76	1.071	0.288	2.303	3.16
4	15	11.18	38.82	38.82	7.65	0.883	0.386	2.708	3.87
5	20	8.82	41.18	41.18	5.29	0.724	0.486	2.996	4.47
6	30	5.88	44.12	44.12	2.35	0.372	0.680	3.401	5.47
7	40	4.71	45.29	45.29	1.18	0.070	0.883	3.689	6.32
8	50	4.12	45.88	45.88	0.59	-0.231	1.090	3.912	7.07
9	60	3.53	46.47	46.47	0.00	-	1.291	4.094	7.74
10	70	3.53	46.47	46.47	0.00	-	1.506	4.248	8.36
11	80	3.53	46.47	46.47	0.00	-	1.722	4.382	8.94
12	90	3.53	46.47	46.47	0.00	-	1.937	4.500	9.48

Table 2. Kinetic data for adsorption of [Acid Violet] =50 ppm onto Cu/AI-LDH at 30 °C to about 90 min

S.No	Time	Final Concentration, Ce	Amount of dye removed, mg/L	Amount of dye removed, mg/g (qt)	qe-qt	log (qe-qt)	t/qt	ln t	$t^{1/2}$
1	0	75.00	0.00	0.00	68.13	1.833	--	--	0.00
2	5	32.50	42.50	42.50	25.63	1.409	0.118	1.609	2.23
3	10	27.50	47.50	47.50	20.63	1.314	0.211	2.303	3.16
4	15	21.25	53.75	53.75	14.38	1.158	0.279	2.708	3.87
5	20	17.50	57.50	57.50	10.63	1.027	0.348	2.996	4.47
6	30	11.25	63.75	63.75	4.38	0.641	0.471	3.401	5.47
7	40	8.75	66.25	66.25	1.88	0.274	0.604	3.689	6.32
8	50	8.13	66.88	66.88	1.26	0.099	0.748	3.912	7.07
9	60	6.88	68.13	68.13	0.00	-	0.881	4.094	7.74
10	70	6.88	68.13	68.13	0.00	-	1.028	4.248	8.36
11	80	6.88	68.13	68.13	0.00	-	1.174312	4.382	8.94
12	90	6.88	68.13	68.13	0.00	-	1.321101	4.500	9.48

Table 3. Kinetic data for adsorption of [Acid Violet] =75 ppm onto Cu/AI-LDH at 30 °C to about 90 min

S.No	Time	Final Concentration, Ce	Amount of dye removed, mg/L	Amount of dye removed, mg/g (qt)	qe-qt	log (qe-qt)	t/qt	ln t	$t^{1/2}$
1	0	100.00	0.00	0.00	87.33	1.941	--	--	0.00
2	5	49.33	50.67	50.67	36.66	1.564	0.099	1.609	2.23
3	10	40.67	59.33	59.33	28.00	1.447	0.169	2.303	3.16
4	15	32.67	67.33	67.33	20.00	1.301	0.223	2.708	3.87
5	20	27.33	72.67	72.67	14.66	1.166	0.275	2.996	4.47
6	30	18.67	81.33	81.33	6.00	0.778	0.369	3.401	5.47
7	40	16.00	84.00	84.00	3.33	0.522	0.476	3.689	6.32
8	50	15.33	84.67	84.67	2.66	0.425	0.591	3.912	7.07
9	60	12.67	87.33	87.33	0.00	-	0.687	4.094	7.74
10	70	12.67	87.33	87.33	0.00	-	0.802	4.248	8.36
11	80	12.67	87.33	87.33	0.00	-	0.916	4.382	8.94
12	90	12.67	87.33	87.33	0.00	-	1.031	4.500	9.48

Table 4. Kinetic data for adsorption of [Acid Violet] =100 ppm onto Cu/AI-LDH at 30 °C to about 90 min

S.No	Time	Final Concentration, Ce	Amount of dye removed, mg/L	Amount of dye removed, mg/g (qt)	qe-qt	log (qe-qt)	t/qt	ln t	$t^{½}$
1	0	50.00	0.00	0.00	47.06	1.673	-	--	0.00
2	5	16.47	33.53	33.53	13.53	1.131	0.149	1.609	2.23
3	10	12.35	37.65	37.65	9.41	0.974	0.266	2.303	3.16
4	15	9.41	40.59	40.59	6.47	0.811	0.370	2.708	3.87
5	20	7.06	42.94	42.94	4.12	0.615	0.466	2.996	4.47
6	30	5.29	44.71	44.71	2.35	0.372	0.671	3.401	5.47
7	40	4.12	45.88	45.88	1.18	0.071	0.872	3.689	6.32
8	50	3.53	46.47	46.47	0.59	-0.230	1.076	3.912	7.07
9	60	2.94	47.06	47.06	0.00	-	1.275	4.094	7.74
10	70	2.94	47.06	47.06	0.00	-	1.488	4.248	8.36
11	80	2.94	47.06	47.06	0.00	-	1.700	4.382	8.94
12	90	2.94	47.06	47.06	0.00	-	1.913	4.500	9.48

Table 5. Kinetic data for adsorption of [Acid Violet] =50 ppm onto Cu/AI-LDH at 40 °C to about 90 min

S.No	Time	Final Concentration, Ce	Amount of dye removed, mg/L	Amount of dye removed, mg/g (qt)	qe-qt	log (qe-qt)	t/qt	ln t	$t^{½}$
1	0	50.00	0.00	0.00	48.24	1.683	-	--	0.00
2	5	14.71	35.29	35.29	12.95	1.112	0.142	1.609	2.23
3	10	10.59	39.41	39.41	8.83	0.946	0.254	2.303	3.16
4	15	7.06	42.94	42.94	5.30	0.724	0.349	2.708	3.87
5	20	4.71	45.29	45.29	2.95	0.469	0.442	2.996	4.47
6	30	2.94	47.06	47.06	1.18	0.072	0.638	3.401	5.47
7	40	2.35	47.65	47.65	0.59	-0.227	0.840	3.689	6.32
8	50	1.76	48.24	48.24	0.00	-	1.037	3.912	7.07
9	60	1.76	48.24	48.24	0.00	-	1.244	4.094	7.74
10	70	1.76	48.24	48.24	0.00	-	1.451	4.248	8.36
11	80	1.76	48.24	48.24	0.00	-	1.659	4.382	8.94
12	90	1.76	48.24	48.24	0.00	-	1.866	4.500	9.48

Table 6. Kinetic data for adsorption of [Acid Violet] =50 ppm onto Cu/AI-LDH at 50 °C to about 90 min

Pseudo-First Order Kinetics

The first order equation is the simplest one and is the most widely used equation for the adsorption of a solute from a solution. The plot is drawn between log (q-q) vs time for different initial concentrations and temperatures for both adsorbents. The value of qe and k_1 is calculated from intercept and slope of the linear plot log (q-q) vs time for different initial concentrations and temperatures. Figure 10 is the plot of log (qe-q) vs time for different initial concentrations by Cu/AI-LDH. The calculated kinetic parameters for concentration and temperature variations for Acid Violet removal by the adsorbent is tabulated in Table 7. The pseudo-first order kinetic model

is poorly fit with adsorption data as the correlation coefficient value (R^3) is low. Hence, the adsorption does not follow first order rate expression.

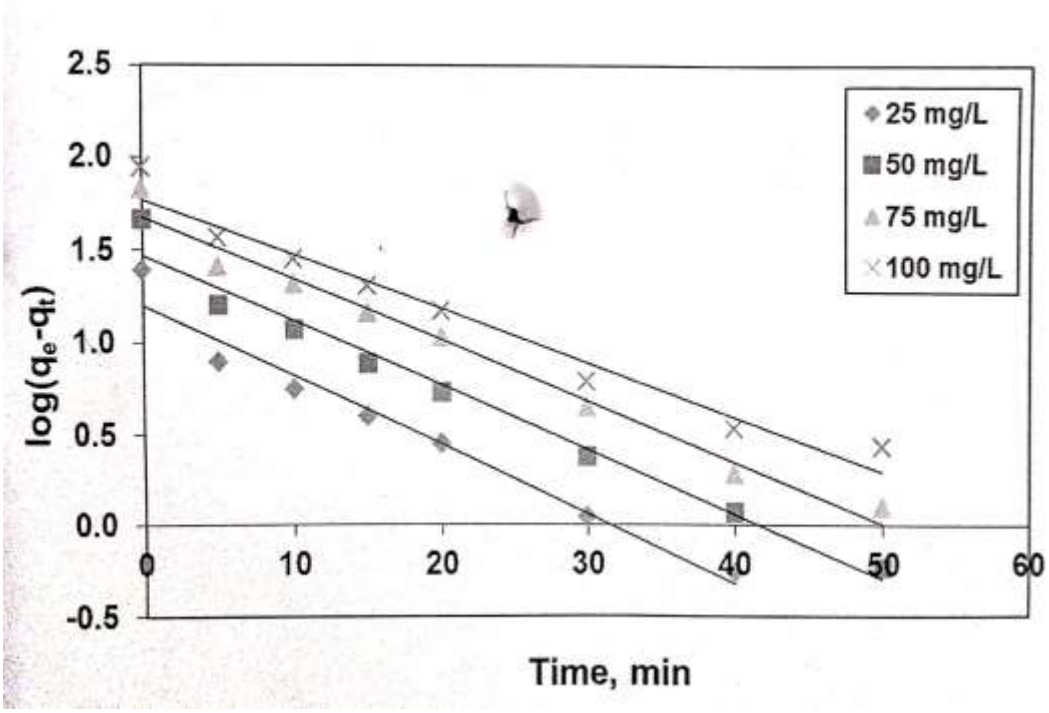

Figure 10. Pseudo first order plot for the adsorption of Acid Violet by Cu/Al-LDH at 30°C

(Concentration variation)

4.6.2 Pseudo Second Order Kinetics

Adsorption of dyes on adsorbent materials has been observed that evolution of the adsorbed amount with time follows second order law

$$\frac{t}{q_t} = \frac{1}{k_2 q_e^2} + \frac{1}{q_e} t \qquad (3)$$

The values of k_2 second order rate constant (g/mg/min) and q_e equilibrium adsorption capacity (mg/g) can be calculated from the plot of t/q, versus t for different initial concentration (shown in Figure 11 and temperature for the adsorbent material. The results of second order plot are given in Table 7(a) and (b). The correlation co-efficient (R^2) values are greater than 0.9994. These result shows that the adsorption of AV dye onto the adsorbent Cu/Al-LDH follows the second order kinetics which describes the adsorption much better than pseudo-first order kinetics. The maximum adsorption capacities q_e calculated from pseudo-second order model for adsorption of TB by Mg/AI-LDH was in accordance with the q_e experimental values. This confirmed that the adsorption obeys pseudo-second order kinetics than the pseudo-first order by the adsorbent. The linear fit of pseudo-second order supported the chemisorption in which the adsorption process is defined by electron exchange or sharing between the adsorbent and adsorbate.

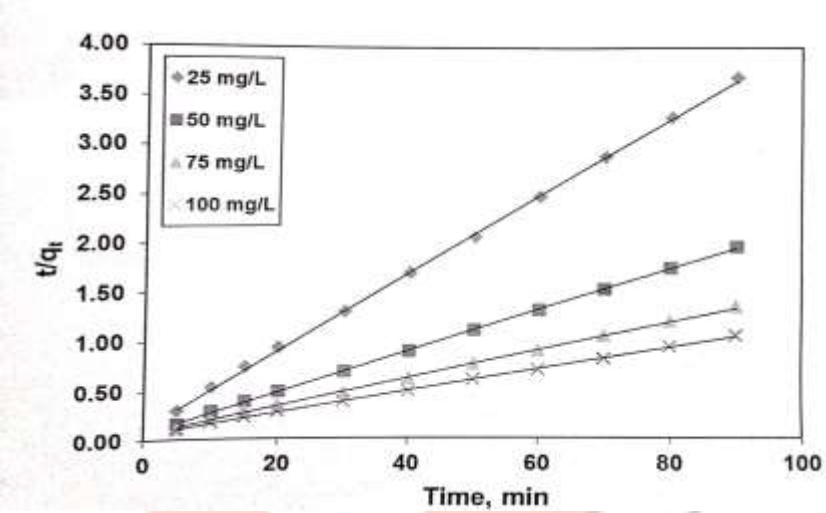

Figure 11. Pseudo second order plot for the adsorption of Acid Violet by Cu/AI-LDH at 30 º

(Concentration variation)

Adsorbents	Cu/AlLDH			
	Initial Concentration(mg/L)			
Parameter	25	50	75	100
q_e exp (mg/g)	24.44	46.47	68.13	87.33
	Pseudo first order kinetics model			
k_1 (min^{-1})	0.077	0.081	0.077	0.069
q_e cal (mg/g)	15.82	29.51	47.96	59.77
R^2	0.9657	0.9779	0.9795	0.9658
	Pseudo second order kinetic model			
k_2 (g/mg min^{-1})	0.0132	0.0062	0.0032	0.0022
h	8.518	14.728	16.694	18.904
q_e cal (mg/g)	25.45	48.54	71.94	92.59
R^2	0.9997	0.9997	0.9994	0.9994

Table .7 (a) Kinetic parameters for the adsorption of AV by Cu/Al-LDH for different initial dye concentration at temperature 30°C

Adsorbents	Cu/Al-LDH		
	Temperature (°C)		
Parameter	30°C	40°C	50°C
q_e exp (mg/g)	**46.47**	**47.06**	**48.24**
	Pseudo first order kinetics model		
k_1 (min^{-1})	0.072	0.078	0.103
q_e cal (mg/g)	29.51	25.13	28.38
R^2	0.9779	0.9557	0.962
	Pseudo second order kinetic model		
k_2 (g/mg min^{-1})	0.0052	0.0079	0.0102
h	14.728	18.762	25.063
q_e cal (mg/g)	48.54	48.78	49.50
R^2	0.9997	0.9999	0.9998

Table.7(b) Kinetic parameters for the adsorption of AV by Cu/Al-LDH at different temperatures (Initial dye concentration = 50mg / L)

4.7 Adsorption isotherm

The adsorption isotherms are generally used for designing the adsorption system. The inear equations of Langmuir and Freundlich isotherms are employed to design the adsorption system of AV by Cu/AL-LDH. The adsorption data for AV dye is encapsulated in Table 8-10.

Initial Concentration, mg. L^{-1}	Final Concentration, Ce, mg. L^{-1}	% Dye Adsorbed	Amount of Dye Adsorbed, q_e, mg. g^{-1}	C_e/q_e	log qe	log Ce	ln Ce	ln qe
10	1.14	88.57	8.86	1.13	0.95	-	-	2.18
20	2.56	87.18	17.44	1.15	1.24	0.41	0.94	2.86
30	4.21	85.96	25.79	1.16	1.41	0.62	1.44	3.25
40	6.11	84.72	33.89	1.18	1.53	0.79	1.81	3.52
50	8.05	83.91	41.95	1.19	1.62	0.91	2.09	3.74
60	10.52	82.47	49.48	1.21	1.69	1.02	2.35	3.90
70	13.24	81.08	56.76	1.23	1.75	1.12	2.58	4.04
80	16.53	79.34	63.47	1.26	1.80	1.22	2.81	4.15
90	18.53	79.41	71.47	1.26	1.85	1.27	2.92	4.27
100	20.13	79.87	79.87	1.25	1.90	1.30	3.00	4.38

Table 8. Isotherm data for adsorption of Acid Violet onto Cu/Al-LDH at 30º to about 90 min

Initial Concentration, mg. L^{-1}	Final Concentration, Ce, mg. L^{-1}	% Dye Adsorbed	Amount of Dye Adsorbed, q_e, mg. g^{-1}	C_e/q_e	log qe	log Ce	ln Ce	ln qe
10	0.88	91.15	9.12	1.10	0.96	-	-	2.21
20	1.95	90.24	18.05	1.11	1.26	0.29	0.67	2.89
30	3.10	89.66	26.90	1.12	1.43	0.49	1.13	3.29
40	4.93	87.67	35.07	1.14	1.54	0.69	1.60	3.56
50	6.82	86.36	43.18	1.16	1.64	0.83	1.92	3.77
60	8.57	85.71	51.43	1.17	1.71	0.93	2.15	3.94
70	10.92	84.40	59.08	1.18	1.77	1.04	2.39	4.08
80	13.45	83.19	66.55	1.20	1.82	1.13	2.60	4.20
90	15.92	82.31	74.08	1.21	1.87	1.20	2.77	4.31
100	18.44	81.56	81.56	1.23	1.91	1.27	2.91	4.40

Table 9. Isotherm data for adsorption of Acid Violet onto Cu/Al-LDH at 40°C to about 90min

Initial Concentration, mg. L^{-1}	Final Concentration, Ce, mg. L^{-1}	% Dye Adsorbed	Amount of Dye Adsorbed, q_e, mg. g^{-1}	C_e/q_e	log qe	log Ce	ln Ce	ln qe
10	0.70	93.04	9.30	1.07	0.97	-	-	2.23
20	1.55	92.25	18.45	1.08	1.27	0.19	0.44	2.92
30	2.50	91.67	27.50	1.09	1.44	0.40	0.92	3.31
40	3.38	91.55	36.62	1.09	1.56	0.53	1.22	3.60
50	5.17	89.66	44.83	1.12	1.65	0.71	1.64	3.80
60	6.60	89.00	53.40	1.12	1.73	0.82	1.89	3.98
70	8.52	87.83	61.48	1.14	1.79	0.93	2.14	4.12
80	10.54	86.82	69.46	1.15	1.84	1.02	2.36	4.24
90	12.86	85.71	77.14	1.17	1.89	1.11	2.55	4.35
100	14.77	85.23	85.23	1.17	1.93	1.17	2.69	4.45

Table 10. Isotherm data for adsorption of Acid Violet onto Cu/Al-LDH at 50°C to about 90min

4.7.1 Langmuir Model

The Langmuir adsorption isotherm was applied to describe the adsorption behavior of Acid Violet (AV) onto the Cu/Al-LDH adsorbent. The plot of C_e/q_e versus C_e for the adsorption of AV by Cu/Al-LDH is shown in Figure 12. The linear form of the Langmuir equation is expressed as:

$$\frac{C_e}{q_e} = \frac{1}{Q_0 b} + \frac{C_e}{Q_0} \quad \text{---------- (4)}$$

where C_e is the equilibrium concentration of the adsorbate (mg L^{-1}), q_e is the amount of adsorbate adsorbed per unit mass of adsorbent at equilibrium (mg g^{-1}), Q_0 is the maximum monolayer adsorption capacity (mg g^{-1}), and b is the Langmuir constant related to the energy of adsorption (L mg^{-1}).

From the experimental data, the plot of C_e/q_e against C_e yielded a straight line, indicating the applicability of the Langmuir model to the adsorption process. The slope and intercept of the linear plot were found to be $1/Q_0$ and $1/(Q_0 b)$, respectively, as illustrated in Figure 12.

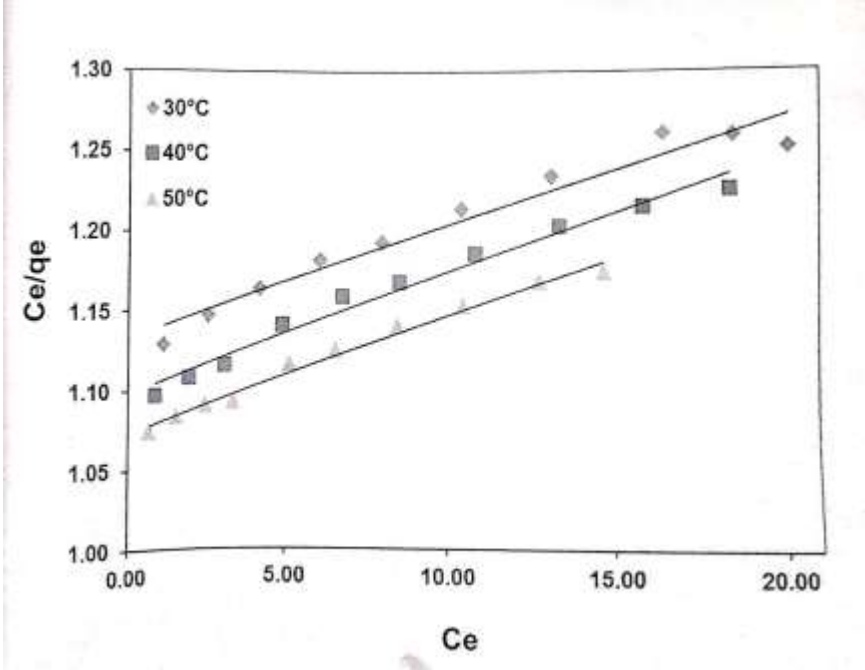

Figure 12. Langmuir adsorption isotherm plot for the adsorption of Acid Violet (AV) onto Cu/Al-LDH.

The Langmuir isotherm parameters calculated from the linear plots are presented in Table 19. The maximum monolayer adsorption capacity (Q_0) and the Langmuir isotherm constant (b) for the adsorption of AV onto Cu/Al-LDH were found to be **144.93 mg g^{-1}** and **0.0061 L mg^{-1}**, respectively, at **30 °C**. The dimensionless separation factor (R_L) for Cu/Al-LDH was found to lie between **0 and 1**, indicating that the adsorption process is favorable. However, the relatively low value of the correlation coefficient (R^2) suggests that the Langmuir model does not provide a completely satisfactory fit to the experimental adsorption data.

4.7.2 Freundlich Model

The Freundlich isotherm is an empirical model used to describe adsorption on heterogeneous surfaces and multilayer adsorption processes. The degree of surface heterogeneity is indicated by the heterogeneity factor $1/n$. The linearized form of the Freundlich isotherm equation is expressed as:

$$\log q_e = \log K_F + \frac{1}{n}\log C_e \quad \text{-------- (5)}$$

where q_e is the amount of adsorbate adsorbed per unit mass of adsorbent at equilibrium (mg g^{-1}), C_e is the equilibrium concentration of the adsorbate (mg L^{-1}), K_F is the Freundlich constant related to adsorption capacity (mg g^{-1})(L $mg^{-1})^{1/n}$, and n is the adsorption intensity parameter.

The values of K_F and n were determined from the intercept and slope, respectively, of the linear plot of $\log q_e$ versus $\log C_e$, as shown in Figure 13.

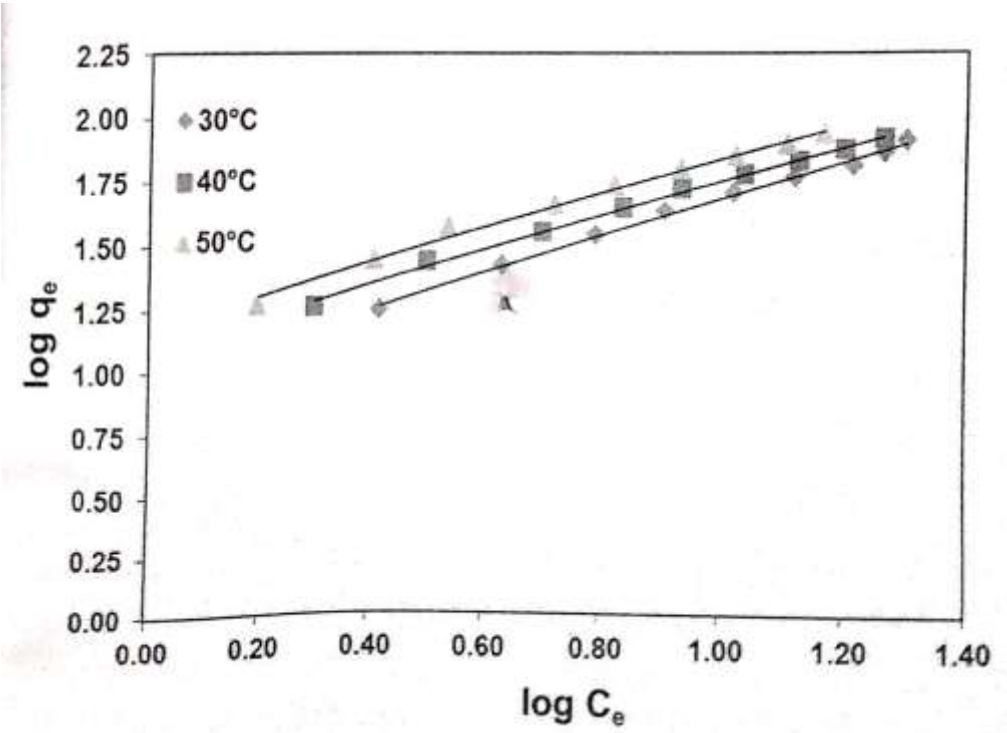

Figure 13. Freundlich adsorption isotherm plot for the adsorption of AV onto Cu/Al-LDH.

The value of the Freundlich adsorption intensity parameter (n) for the adsorption of AV dye onto Cu/Al-LDH was found to be greater than one, indicating that the adsorption of AV by the adsorbent material was favorable. Moreover, The equilibrium data fitted the Freundlich isotherm with a high correlation coefficient value (R^2). The much higher correlation coefficient value for the Freundlich isotherm predicts heterogeneity and multilayer adsorption of AV onto Cu/Al-LDH.

ample	Temperature °C	Isotherm Models						
		Langmuir				Freundlich		
		Q_0	b	R_L	R^2	n	k_f	R^2
u/Al-LDH	30	144.93	0.0061	0.7666	0.9568	1.416	9.256	0.9961
	40	133.33	0.0068	0.7454	0.9796	1.525	12.229	0.9971
	50	138.89	0.0067	0.7488	0.988	1.529	15.035	0.9908

Table.11 Isotherm parameters for adsorption of AV by Cu/Al-LDH

4.8 Adsorption Thermodynamics

Thermodynamic parameters such as Gibbs free energy change (ΔG°), enthalpy change (ΔH°), and entropy change (ΔS°) of adsorption were calculated using the binding constant obtained from the Langmuir equation, according to the following relations:

$$\Delta G^\circ = -RT\ln K_c \text{ ------- 6}$$

$$\ln K_c = \frac{\Delta S^\circ}{R} - \frac{\Delta H^\circ}{RT} \text{ ------- 7}$$

The enthalpy change (ΔH°) was calculated from the slope of the linear plot of $\ln K_c$ versus $1/T$, as shown in Figure 14. The negative value of ΔG° indicates a high affinity of the dye towards the surface of Cu/Al-LDH, and confirms that the adsorption process is favorable and spontaneous in nature. The enthalpy change (ΔH°) is used

to distinguish between chemical and physical adsorption. The calculated thermodynamic parameters are presented in Table 12.

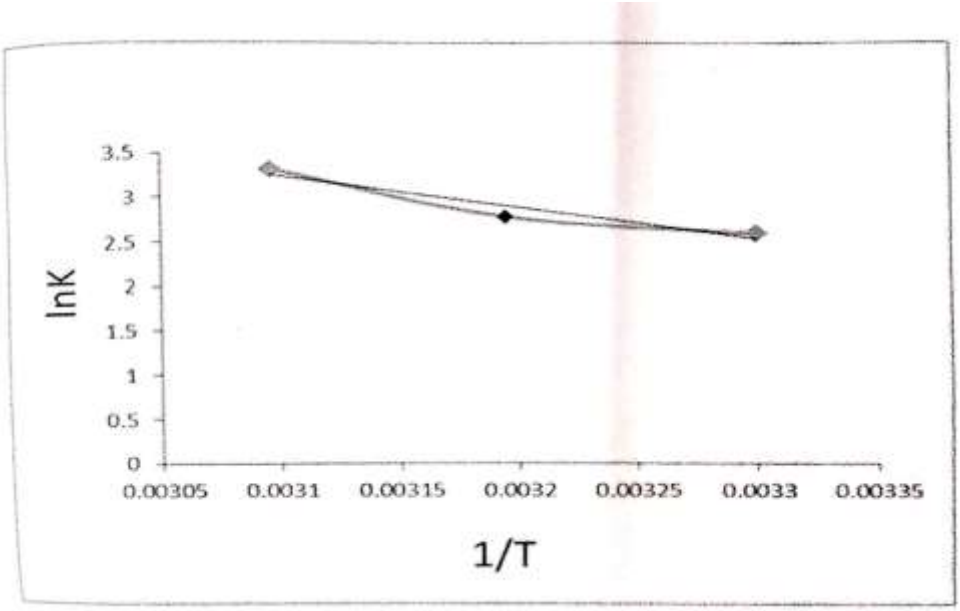

Figure 14. Van't Hoff's plot for the adsorption of AV by Cu/Al-LDH

Adsorbent	Initial concentration of [AV] mg/l	ΔG° (KJ/mol)			ΔH° (KJ/mol)	ΔS° (J/K/mol)
		303K	313K	323K		
Cu/AlC-LDH	25	-9.51	-7.22	-8.89	30	119
	50	-6.49				
	75	-5.78				
	100	-4.86				

Table. 12 Thermodynamic parameters from Van't Hoff plots for the adsorption of AV by Cu/Al-LDH at different temperature

The enthalpy change (ΔH°) calculated for the adsorbent Cu/Al-LDH (30 kJ mol^{-1}) is below 80 kJ mol^{-1}, revealing that the adsorption process is physisorption. The positive entropy change (ΔS°) values indicate an increase in randomness at the solid–solution interface during the adsorption process.

V. CONCLUSION

The present study substantiates the successful preparation of Cu/Al-LDH by the co-precipitation method and its suitability as an adsorbent for the removal of Acid Violet (AV) from aqueous solution. From the investigation, the following conclusions were drawn:

1. The maximum adsorption capacity for the removal of Acid Violet onto Cu/Al-LDH was found to be 144.93 mg g^{-1} at 30 °C, demonstrating that the prepared material is highly efficient for AV removal from aqueous solution.
2. An acidic pH of 3 was found to be the optimum condition for maximum adsorption, with approximately 90% removal observed for 50 mg L^{-1} AV dye solution.

3. The adsorption kinetics of AV onto Cu/Al-LDH were best described by the pseudo-second-order kinetic model, which showed a higher correlation coefficient compared to the pseudo-first-order model. The equilibrium data were analyzed using both Langmuir and Freundlich isotherm models.

4. The pseudo-second-order kinetic model exhibited the best fit for kinetic data, while the isotherm results indicated heterogeneous and multilayer adsorption, as described by the Freundlich model.

5. The adsorption of AV increased with an increase in temperature from 30 °C to 50 °C, indicating that the adsorption process is endothermic in nature. This observation is further supported by the positive value of enthalpy change (ΔH°).

6. Thermodynamic analysis revealed that the adsorption of AV onto Cu/Al-LDH is favorable and spontaneous, as indicated by the negative values of Gibbs free energy change (ΔG°, ranging from –4.86 to –9.51 kJ mol^{-1}). The positive enthalpy change ($\Delta H^\circ = 30$ kJ mol^{-1}) confirms the endothermic nature of the process and suggests physisorption ($\Delta H^\circ < 80$ kJ mol^{-1}). The positive entropy change (ΔS°) indicates increased disorder at the solid–liquid interface during adsorption.

These results emphasize that the prepared Cu/Al-LDH is a promising and effective adsorbent for the removal of Acid Violet from aqueous solutions.

REFERENCES

1. Farghali, M. A., Selim, A. M., Khater, H. F., Bagato, N., Alharbi, W., Alharbi, K. H., Radwan, I. T. Optimized adsorption and effective disposal of Congo Red dye from wastewater: Hydrothermal fabrication of MgAl-LDH nanohydrotalcite-like materials. *Arabian Journal of Chemistry*, **15** (2022), 104171.
2. Brahma, D., Saikia, H. S. Synthesis of ZrO_2/MgAl-LDH composites and evaluation of isotherm, kinetics, and thermodynamic properties in the adsorption of Congo Red dye. *Chemical Thermodynamics and Thermal Analysis*, **7** (2022), 100067.
3. El Mersly, L., El Mouchtari, E. M., Moujahid, E. M., Forano, C., El Haddad, M., Briche, S., Tahiri, A. A., Rafqah, S. ZnCr-LDHs with dual adsorption and photocatalysis capability for the removal of Acid Orange 7 dye in aqueous solution. *Journal of Science: Advanced Materials and Devices*, **6** (2021), 118–126.
4. Meili, L., Lins, P. V., Zanta, C. L. P. S., Soletti, J. I., Ribeiro, L. M. O., Dornelas, C. B., Silva, T. L., Vieira, M. G. A. MgAl-LDH/Biochar composites for methylene blue removal by adsorption. *Applied Clay Science*, **168** (2019), 11–205.
5. Mohamed, F., Abukhadra, M. R., Shaban, M. Removal of safranin dye from water using polypyrrole nanofiber/Zn–Fe layered double hydroxide nanocomposite with enhanced adsorption and photocatalytic properties. *Science of the Total Environment*, **640–641** (2018), 352–363.
6. Khodam, F., Rezvani, Z., Amani-Ghadim, A. R. Enhanced adsorption of Acid Red 14 by co-assembled LDH/MWCNTs nanohybrid: Optimization, kinetic and isotherm studies. *Journal of Industrial and Engineering Chemistry* (2014).
7. Zheng, Y., Cheng, B., You, W., Yu, J., Ho, W. 3D hierarchical GO–NiFe LDH composite with enhanced adsorption affinity toward Congo Red, Methyl Orange, and Cr(VI) ions. *Journal of Hazardous Materials*, **369** (2019), 214–225.
8. Hu, H., Liu, J., Xu, Z., Zhang, L., Cheng, B., Ho, W. Hierarchical porous Ni/Co-LDH hollow dodecahedron with adsorption properties for Congo Red and Cr(VI) ions. *Applied Surface Science*, **478** (2019), 981–990.
9. Pourfaraj, R., Fatemi, S. J., Kazemi, S. Y., Biparva, P. Synthesis of hexagonal mesoporous MgAl-LDH nanoplatelets as an adsorbent for the effective adsorption of Brilliant Yellow. *Journal of Colloid and Interface Science* (2017). DOI: 10.1016/j.jcis.2017.07.101

10. Mamat, M., Abdullah, M. A. A., Jaafar, A. M., Soh, S. K. C., Lee, C. E. Removal of Methyl Orange dye by manganese–aluminium layered double hydroxide. *ASM NG Journal*, Special Issue AIMS2018, **1** (2018), 105–113.
11. Zhou, L., Liu, J., Lu, A., Shen, J., Xu, J., Jiang, H. Controllable synthesis of cubic magnetic $MgFe_2O_4$ derived from MgFe-LDH for efficient removal of Methyl Orange. *Chemical Engineering Journal*, **428** (2022), 131174.
12. Zubair, M., Aziz, H. A., Ihsanullah, Ahmad, M. A., Al-Harthi, M. A. Biochar-supported CuFe layered double hydroxide composite as a sustainable adsorbent for efficient removal of anionic azo dye from water. *Environmental Technology & Innovation*, **23** (2021), 101614.
13. Wang, H., Zhao, W., Chen, Y., Li, Y. Nickel–aluminium layered double oxides modified magnetic biochar from waste corncob for efficient removal of Acridine Orange. *Bioresource Technology*, **315** (2020), 123834.
14. Iqbal, M. M., Imran, M., Hussain, T., Naeem, M. A., Al-Kahtani, A. A., Shah, G. M., Ahmad, S., Farooq, A., Rizwan, M., Majeed, A., Khan, A. R., Ali, S. Effective sequestration of Congo Red dye with ZnO/cotton stalk biochar nanocomposite: Modeling, reusability, and stability. *Journal of Saudi Chemical Society*, **25** (2021), 101176.
15. Rubangakene, N. O., Elwardany, A., Fujii, M., Sekiguchi, H., Elkady, M., Shokry, H. Biosorption of Congo Red dye from aqueous solutions using pristine biochar and ZnO-biochar from green pea peels. *Chemical Engineering Research and Design*, **189** (2023), 636–651.
16. Zhao, X., Wang, J., Liu, Y. LDHs and the reuse of adsorbent sludge as a nanofiller for polypropylene. *Journal of Alloys and Compounds*, **587** (2014), 99–104.
17. Quassif, H., Moujahid, E. M., Lahkale, R., Sadik, R., Bouragba, F. Z., Sabbar, E. M., Diouri, M. Zinc–aluminum layered double hydroxide: Highly efficient removal of tartrazine dye from aqueous solution by adsorption. *Surfaces and Interfaces* (2019).
18. Shan, R.-R., Yan, L.-G., Yang, K., Yu, S.-J., Hao, Y.-F., Yu, H.-Q., Du, B. Magnetic Fe_3O_4/MgAl-LDH composite for effective removal of three red dyes from aqueous solution. *Chemical Engineering Journal* (2014).
19. Anthonysamy, S. I., Ahmad, M. A., Khan, N., Yahaya, E. M. Insight into the mechanism of Mg/Al-LDH supported on rubber seed shell biochar for Remazol Brilliant Violet SR removal. *Arabian Journal of Chemistry*, **16** (2023), 104643.
20. Chen, Y., Jing, C., Zhang, X., Jiang, D., Liu, X., Dong, B., Feng, L., Li, S., Zhang, Y. Acid-salt-treated CoAl-LDH nanosheets with enhanced adsorption capacity for Methyl Orange dye. *Journal of Colloid and Interface Science*, **548** (2019), 100–109.
21. Santos, R. M. M. dos, Gonçalves, R. G. L., Constantino, V. R. L., Santilli, C. V., Borges, P. D., Tronto, J., Pinto, F. G. Adsorption of Acid Yellow 42 dye on calcined layered double hydroxides: Effect of time, concentration, pH, and temperature. *Applied Clay Science*, **140** (2017), 132–139.

Preparation Of Copper Zinc Tin Selenide ($Cu_2znsnse_4$) Quaternary Chalcogenide Nanoparticles For Energy Conversion Applications

Dhivya R

Head, Assistant Professor

Department of Chemistry

Sri Sarada Niketan College of Science for Women, Karur, India.

Abstract

Thin-film solar cell technologies such as $Cu(In,Ga)(S,Se)_2$ (CIGS) and CdTe have demonstrated high power conversion efficiencies; however, their large-scale commercialization is hindered by the toxicity, scarcity, and high cost of constituent elements. In this context, copper-based quaternary chalcogenide semiconductors, particularly Cu_2ZnSnS_4 (CZTS) and $Cu_2ZnSnSe_4$ (CZTSe), have emerged as promising alternative absorber materials due to their earth-abundant, low-cost, and environmentally benign nature. These materials exhibit suitable direct band gaps, high absorption coefficients, and intrinsic p-type conductivity, making them well suited for photovoltaic applications. Despite their favorable properties and a high theoretical efficiency limit, the practical performance of CZTS/CZTSe solar cells is currently limited by issues such as open-circuit voltage deficit, narrow compositional stability, secondary phase formation, and intrinsic defect disorder. This work summarizes the fundamental properties, crystal structure, phase stability, defect chemistry, deposition techniques, and applications of CZTSe-based thin films, highlighting current challenges and future prospects for improving device performance and achieving commercial viability.

Key words

CZTS, CZTSe, Thin-film solar cells, Kesterite structure, Earth-abundant materials, Absorber layer, Defect chemistry, Photovoltaics

I. INTRODUCTION

Nano science is the emerging science of objects that intermediate in size between the largest molecules and the smallest structure that can be fabricated by very smallest dimensions ranging from nanometers less than 100 nanometers. In chemistry, tlas range of sine has historically been associated with colloids, miceltes. Polymer molecules, phase-separated regions in block copolymers and similar structure-typically and very large molecules or aggregates of many molecules. More recently structure such as Bucky tubes, silicon nano rods and compound semiconductor quantum dots have emerged as particularly interesting classes of nanostructure. A scale of relative dimensions of various objerts was given in figure 1 In physics electrical engineering, nanoscience is most often associated with quantum behavior, and the behavior of electrons and photons in nano scale structures. Biology and biochemestry also have a deep interest in nanostructure as components of cell, many of the most interesting structures in biology from-DNA and viruses to sub cellular organ cells and gap junction can be considered as nanostructures. These are very small structures are interesting for many reasons

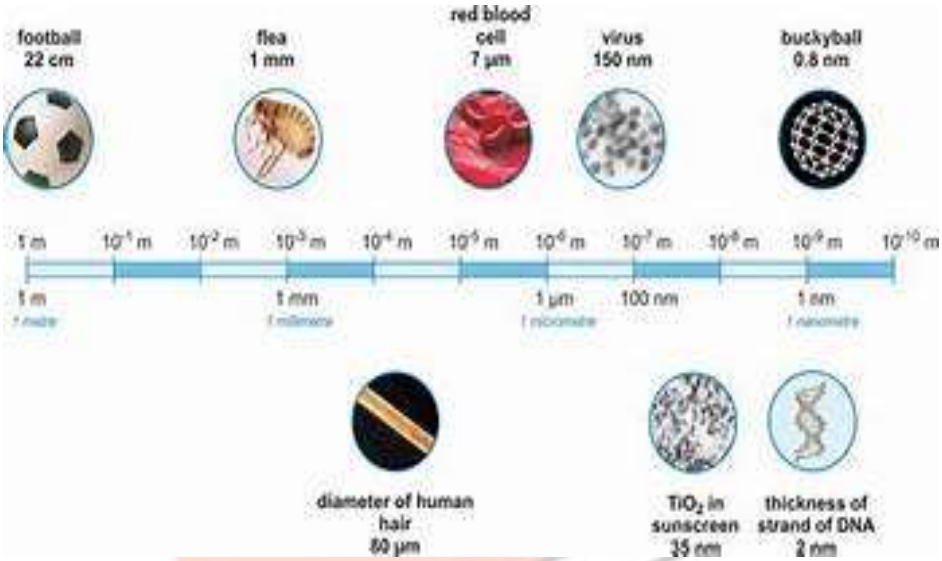

Figure.1 A Scale of Relative Dimensions of Various Objects

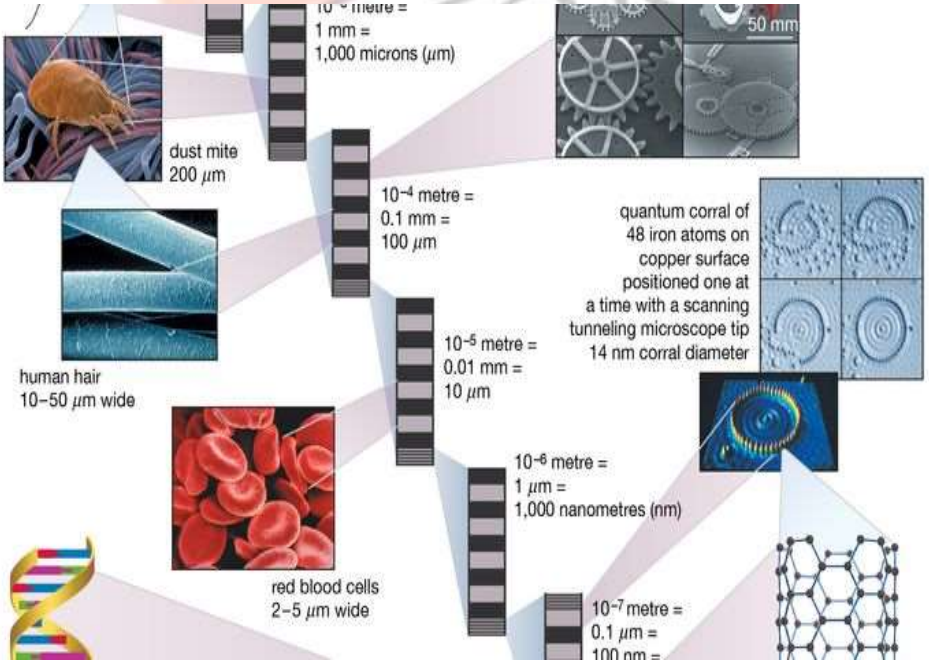

Figur.2 Examples from Biological and Mechanical realms illustrate various orders of magnitude

Because many nanoscale structures have been in-accessible and off the beaten scientific track, studying these structures leads to new wonders. Very small particles, or large, ordered, aggregate of molecules or atoms, are simply not structure that science has been able to explore carefully. Figure 2 shows some examples of biological and mechanical realms which illustrates various orders of magnitude. Nanostructures are in range of sizes in which quantum phenomenon-especially to be entanglement and other reflections of the wave structure character of matter would be expected to be important [4-8] Quantum phenomena are of course, the ultimate basis of the properties of atoms and molecules, but are largely hidden behind the classical behavior in macroscopic matter and structure Quantum dots and nanowires have already been prepared and demonstrated to show remarkable electronic properties; there will, 1 am certain, be other nanoscale materials, and other properties, to study and exploit it.

When describing a nanomaterial it is therefore important to describe not only the mean particle size but also the size of the primary particles. In addition, information on the presence of agglomerates and/or aggregates should be presented. When the mean particle size deviates (Le. is larger) from the primary particle size this would indicate the presence of agglomerates/aggregates. This information should be included in the description of the nanomaterial and/or the product containing the nanomaterial. In addition to size, the specific surface area is a good metric to describe particulates. The specific surface area as determined by the BET method has the advantage of being independent of the primary versus the agglomerated state.

II. AIM AND OBJECTIVE OF THE STUDY

The aim of this study is to investigate $Cu_2ZnSnSe_4$ (CZTSe) as an earth-abundant, low-cost, and environmentally benign absorber material for thin-film solar cell applications, while identifying the key factors that limit its photovoltaic performance. The objectives include understanding the motivation for replacing conventional CIGS and CdTe absorbers, analyzing the crystal structure and phase stability of CZTSe, examining the influence of stoichiometry and secondary phase formation, evaluating intrinsic defects and defect complexes responsible for open-circuit voltage deficit, reviewing vacuum and non-vacuum thin-film deposition techniques, assessing recent progress in CZTSe-based solar cell efficiencies, and exploring potential applications of CZTSe beyond photovoltaics.

III. Cu_2ZnSnS_4 (CZTS) and $Cu_2ZnSnSe_4$ (CZTSe)

Thin-film solar cell technologies such as $Cu(In,Ga)(S,Se)_2$ (CIGS) and CdTe have achieved power conversion efficiencies (PCEs exceeding 22%, demonstrating their strong potential to replace crystalline silicon. However, their large-scale deployment is restricted by the toxicity, scarcity, and high cost of elements such as In, Ga, Cd, and Te. These concerns necessitate the development of alternative absorber materials that are environmentally benign, earth-abundant, and economically sustainable.

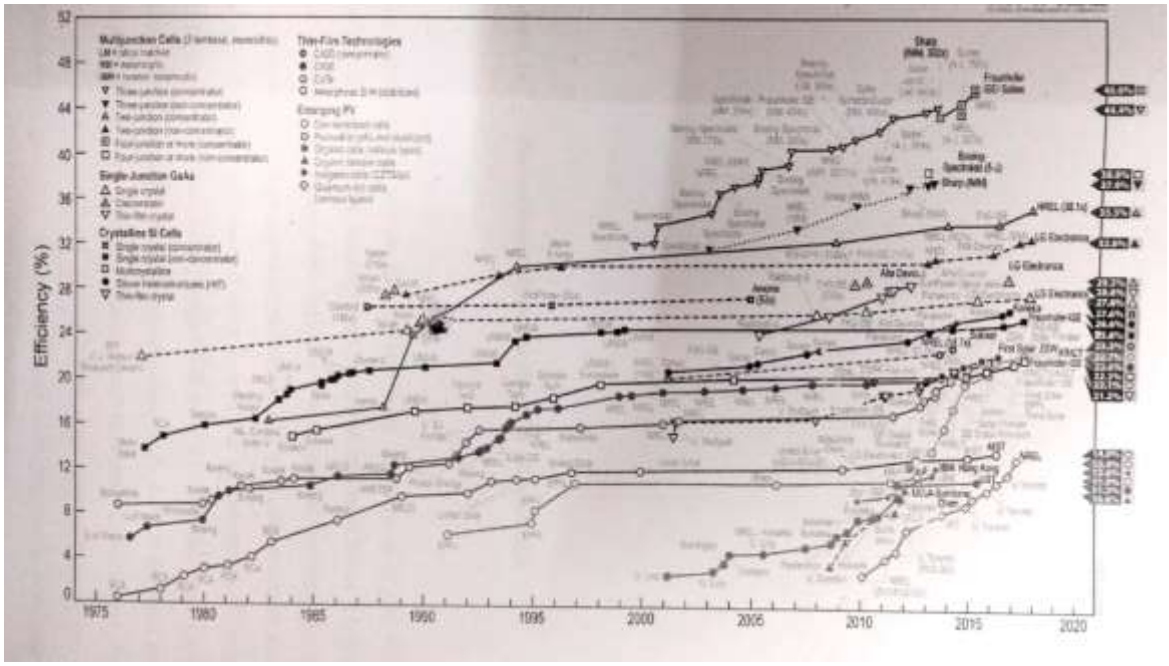

Figure.3 Photovoltanics Efficiency Chart for all Solar Cells

3.1 Role of the Absorber Layer

The absorber layer is the most critical component of a thin-film solar cell, as it governs light absorption, charge carrier generation, and charge separation. Although CIGS and CdTe exhibit excellent optoelectronic properties, their environmental and economic drawbacks limit their long-term viability. Therefore, identifying a low-cost and non-toxic absorber material with comparable properties is essential.

3.2 CZTS and CZTSe as Promising Absorbers

Copper-based quaternary chalcogenide semiconductors such as CZTS, CZTSe, and CZTSSe have emerged as strong alternatives to conventional thin-film absorbers. These I–II–IV–VI materials possess suitable direct band gaps, high absorption coefficients, and intrinsic p-type conductivity. Their constituent elements are abundant and non-toxic, making them ideal candidates for sustainable photovoltaic applications.

Absorber Material Properties	**Desirable Requirement**	**CZTSe**
Crystal structure	Stable, defect-tolerant	Kesterite
Optical band gap	1.1 – 1.6 eV	1.3 – 1.5 eV
Absorption coefficient	$\geq 10^4$ cm^{-1}	$> 10^4$ cm^{-1}
Conductivity type	p-type	p-type
Carrier concentration	$10^{15} – 10^{18}$ cm^{-3}	$10^{16} – 10^{18}$ cm^{-3}
Carrier mobility	> 1 cm^2 V^{-1} s^{-1}	~1–10 cm^2 V^{-1} s^{-1}
Elemental abundance	Earth-abundant	Cu, Zn, Sn, Se
Toxicity	Non-toxic	Non-toxic
Deposition compatibility	Simple, scalable	Vacuum & solution-based
Theoretical PCE	≥ 30%	~32.2%
Best reported PCE	≥ 19% (commercial target)	12.6%

Table 1.1 Material Properties of CZTSe as an absorber layer

3.3 Efficiency Potential and Research Progress

Shockley–Queisser limit calculations predict a theoretical efficiency of approximately 32.2% for CZTSSe absorbers. Since the first CZTS-based solar cell reported by Katagiri et al. in 2001, research on these materials has grown rapidly. Despite significant progress, the highest reported efficiency remains at 12.6%, which is below the threshold required for commercial manufacturing.

3.4 Open-Circuit Voltage Deficit

One of the major challenges in CZTSe and CZTSSe solar cells is the large open-circuit voltage (V_oc) deficit, typically below 500 mV. This deficit arises from intrinsic defects, Cu–Zn disorder, secondary phase formation, and absorber decomposition during high-temperature processing, particularly at the Mo back contact interface.

3.5 Crystal Structure of CZTSe

CZTSe crystallizes in a tetragonal structure derived from chalcopyrite $CuInSe_2$, with Zn and Sn replacing In in a 1:1 ratio. It can form either kesterite or stannite structures, with kesterite being thermodynamically more stable and preferred for photovoltaic applications. Due to the similar electronic properties of Cu and Zn, distinguishing these phases using conventional X-ray diffraction is challenging.

3.6 Phase Diagram and Stoichiometry

The formation of phase-pure CZTSe is difficult because of its narrow thermodynamic stability region. Small deviations in stoichiometry can result in secondary phases such as ZnSe, Cu_2Se, or SnSe, which negatively affect device performance. Experimental studies show that Cu-poor and Zn-rich compositions lead to higher efficiencies, though excessive Zn can promote ZnSe formation.

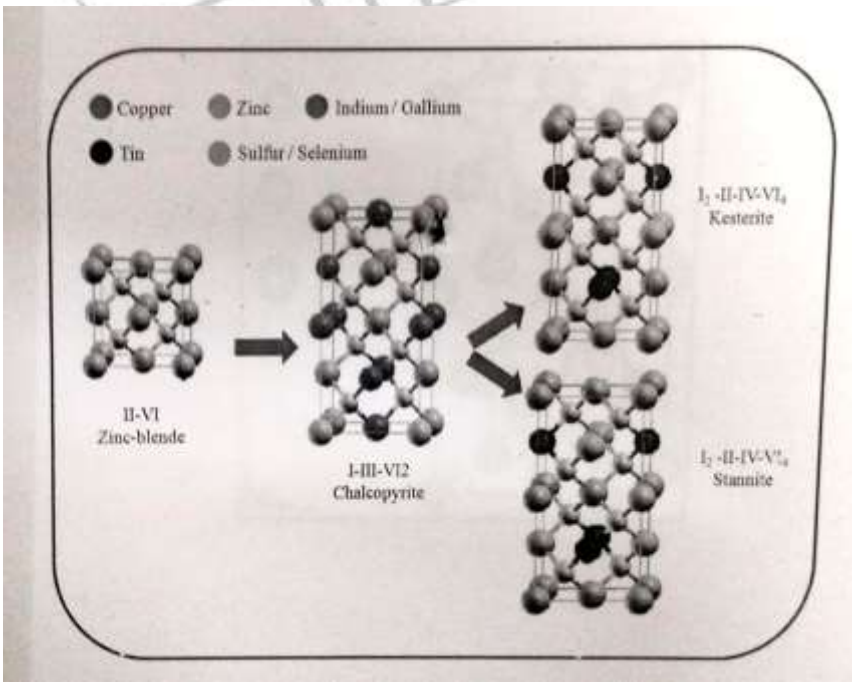

Figure.4 Evolution of CZTSe from Zinc-Blende System

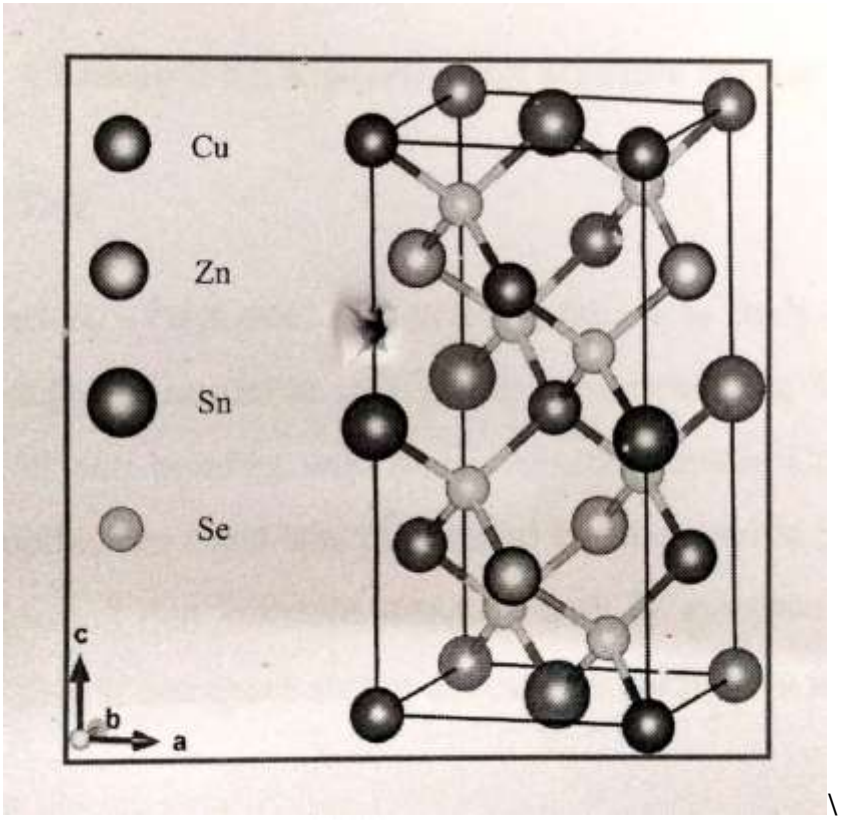

\

Figure.5 The Conventional Tetragonal Structure of CZTSe

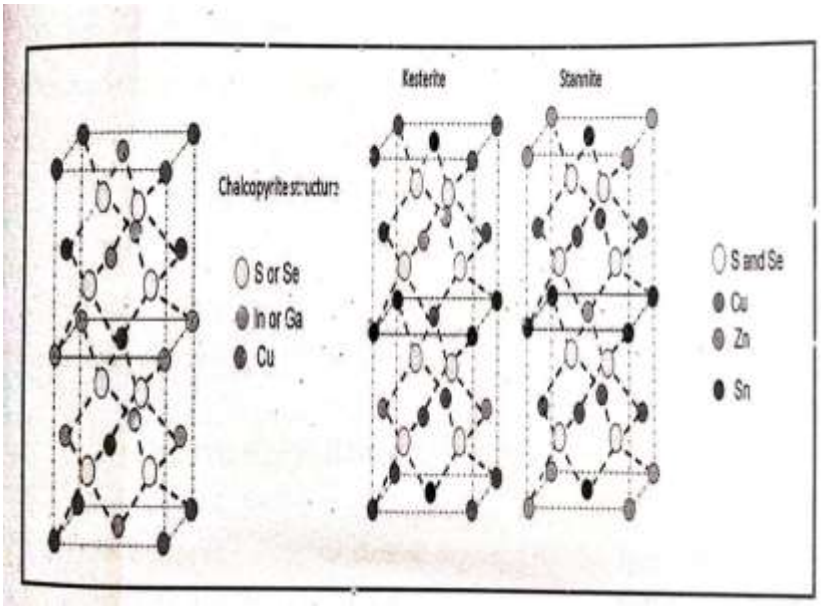

Figure.6 Chalcopyrite, Kesterite and Stannite Crystal Structures

3.7 Defects in CZTSe

Intrinsic point defects, including Cu vacancies and Cu–Zn antisites, dominate the defect chemistry of CZTSe. While Cu vacancies contribute to p-type conductivity, defect clusters and disorder increase recombination losses and reduce V_oc. Order–disorder transitions can alter the effective band gap by more than 100 meV, significantly impacting device performance.

3.8 Thin-Film Deposition Techniques

CZTSe thin films have been fabricated using a wide range of vacuum-based and non-vacuum-based techniques, including sputtering, thermal evaporation, pulsed laser deposition, electrochemical deposition, sol–gel processing, and nanoparticle ink methods. Solution-based techniques are particularly attractive due to their low cost and scalability.

3.9 Nanocrystal-Based CZTSe

CZTSe nanocrystals synthesized via hot-injection methods exhibit suitable band gaps (~1.5 eV) for photovoltaic applications. Solar cells fabricated using nanoparticle inks have achieved efficiencies up to 7.2% after selenization, although interfacial carbon layers and defect-related recombination remain challenges.

3.10 Applications of CZTSe

Beyond photovoltaics, CZTSe finds applications as a counter electrode in dye-sensitized and organic solar cells, a hole transport material, an electrode material for lithium-ion batteries and supercapacitors, a catalyst for hydrogen production and wastewater treatment, and a functional material in resistive memory devices.

IV. EXPERIMENTAL METHODS

4.1 Introduction

In recent years, nanoscience and nanotechnology have emerged as major interdisciplinary research fields integrating physics, chemistry, materials science, engineering, and biology. This progress has been driven by the development of advanced experimental tools capable of probing material properties at near-atomic resolution. At the nanoscale, materials exhibit unique physical, chemical, and optical properties that differ significantly from their bulk counterparts, motivating the fabrication of nanomaterials with enhanced or novel functionalities. These materials have found applications in electronics, optoelectronics, catalysis, diagnostics, and energy conversion. Nanomaterials can exist as powders, colloidal suspensions, or embedded in solid matrices, and their properties depend not only on composition and size but also on shape and synthesis route.

4.2 Synthesis of Nanoparticles in Solution

The synthesis of nanoparticles in solution is a widely used wet-chemical method that involves the thermal decomposition or chemical reaction of precursors in a high-boiling coordinating solvent. Upon injection of precursors into a heated reaction flask, supersaturation is achieved, leading to nucleation once a critical concentration threshold is exceeded. This process results in the formation of nanocrystal nuclei, followed by controlled growth as precursors continue to supply material to the particle surface.

Nanoparticle growth is governed by parameters such as precursor concentration, reaction temperature, and time. Higher temperatures generally enhance atom diffusion and growth rates. To stop growth at a desired size, the

reaction can be rapidly quenched by cooling the solution. Nanoparticles are subsequently isolated by adding a solvent that is miscible with the reaction medium but incompatible with the surface ligands.

4.3 Role of Surfactants and Shape Control

Surfactants play a crucial role in stabilizing nanoparticles during synthesis by preventing agglomeration and controlling surface energy. Selective binding of surfactants to specific crystallographic facets enables shape control, allowing the formation of nanostructures such as dots, rods, tetrapods, and disks. The use of multiple surfactants with different binding strengths further enhances anisotropic growth and morphological control.

4.4 Advantages of Solution-Based Synthesis

Solution-based synthesis offers several advantages, including low cost, scalability, and precise control over nanoparticle size, shape, and composition. It enables the preparation of a wide range of materials, including metals, semiconductors, insulators, alloys, and doped systems, with sizes ranging from a few nanometers to several hundred nanometers. Additionally, this method allows the production of nanoparticles with narrow size distributions, which is essential for uniform optical and electronic properties.

4.5 Other Synthesis Techniques

Apart from solution-based methods, nanomaterials can also be synthesized using sol–gel processing, physical and chemical vapor deposition, and hydrothermal techniques. Each method offers specific advantages depending on the desired material properties, morphology, and application requirements.

4.6 Characterization Techniques

The synthesized nanomaterials are characterized using various techniques to evaluate their structural, morphological, and optical properties. X-ray diffraction (XRD) is employed to determine crystal structure and phase purity, scanning electron microscopy (SEM) and transmission electron microscopy (TEM) are used to analyze surface morphology and particle size, and UV–Visible spectroscopy is used to study optical absorption characteristics.

V. RESULTS AND DISCUSSION

In this chapter, the microstructural and optical properties of the synthesized **CZTSe** nanoparticles are discussed in detail. Characterization results obtained from various experimental techniques such as X-ray diffraction (XRD), scanning electron microscopy (SEM), transmission electron microscopy (TEM), and UV–Vis spectrometry are given below.

5.1 GROWTH MECHANISM OF CZTSe

The formation of a quaternary and multinary chalcogenide compound is quite difficult when compared with other kinds of nanomaterials, because it contains a number of controlled hydrothermal reaction parameters. As we know, the hydrothermal method is suitable for multiple-element-containing nanomaterials due to its potential influence of reaction parameters. Hydrothermal reaction period, solvent, temperature, and pressure are the key components for the successful synthesis of nanomaterials using the hydrothermal method.

$$Cu_2Se + ZnSnSe \rightarrow Cu_2ZnSnSe$$

Growth mechanism of CZTSe nanoparticles

CZTSe nanoparticles are formed when the precursor materials react in an aqueous solution, and the corresponding metal selenides are easily bonded with binary and ternary selenides. Finally, this reaction yields a quaternary metal selenide, namely the CZTSe compound. A ternary ZnSnSe compound reacts with a binary Cu_2Se phase to form CZTSe. This process is clearly illustrated in this equation.

5.2 PHASE IDENTIFICATION USING XRD

In addition to the investigation of spurious phase formation in CZTSe nanoparticles, powder XRD analysis was performed. A detailed examination of the CZTSe samples was carried out. All diffraction peaks appear to correspond mainly to the kesterite phase. However, a few extra peaks are also present in the diffraction patterns. Overall, the particles seem to be composed predominantly of the kesterite structure. No textured preferred orientation, if present, is weak. Two additional small peaks, more resembling 2D diffraction bands, are present near the (112) most intense peak. This is a possible indication of the presence of stacking faults in the structure. Some small extra peak is observed, with a line width compatible with that of the kesterite reflections. The peak at low angle is compatible with a 2×2 kesterite supercell, although this might just be a coincidence. The powder diffraction information from a thin film is not sufficient for a structural determination. It would therefore be interesting to be able to synthesize some more material and to perform a detailed diffraction analysis. The position is not compatible with any possible known selenide of the reacting species. Two major extra peaks are present in the diffraction pattern of kesterite. The broadening is larger, so we can assume that those peaks belong to a second phase [12,16,24,56]. The presence of just two reflections, multiple orders of the same diffraction signal, indicates a possible strong texture (presumably of fiber type) of this second phase. Data are not enough for drawing any conclusions based on the present measurements alone, but peak positions are compatible with those of SnS ((h k 0) reflections of orthorhombic SnSe).

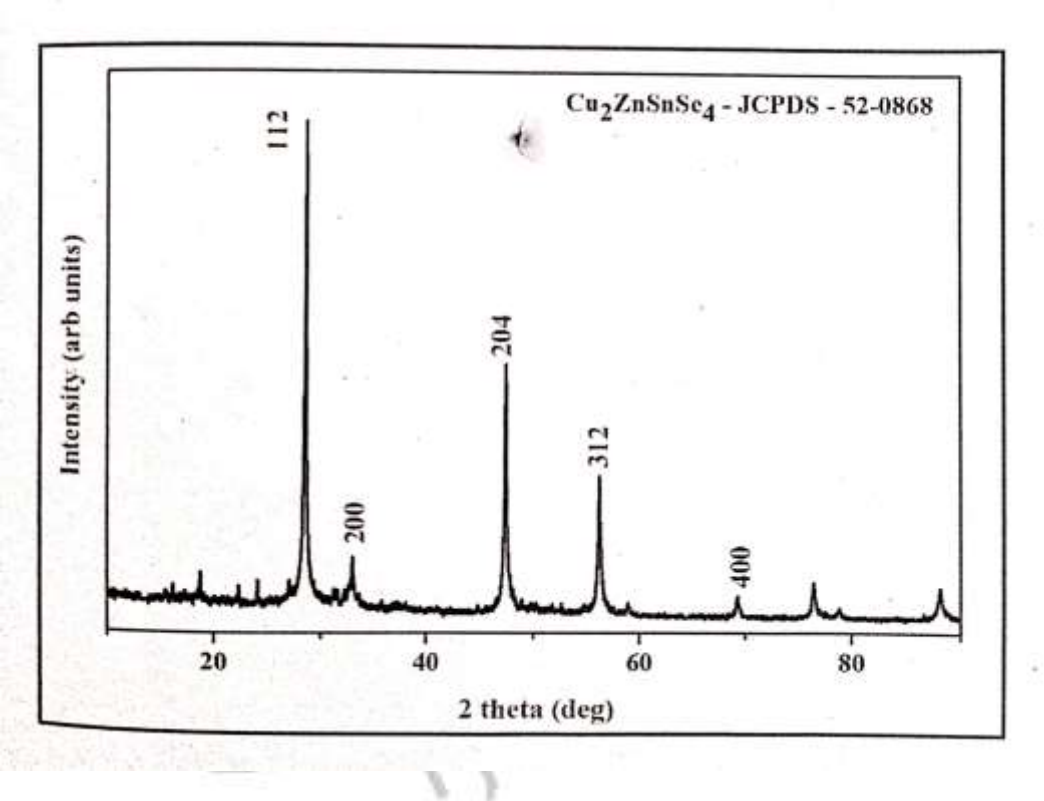

Figure 7 . PXRD pattern of synthesized CZTSe nanoparticles

The discrepancy in the relative peak intensities with the standard diffraction pattern of the CZTSe may be attributed due to the fact that the spherical nanoparticles likely have preferred growth orientations. Moreover, the relative peak intensities of the (112) to (204) in our case are quite same with earlier report which Implies that the CZTSe nanoparticles fabricated by different methods exhibit different preferred orientations

5.3 MORPHOLOGY INVESTIGATION BY SEM

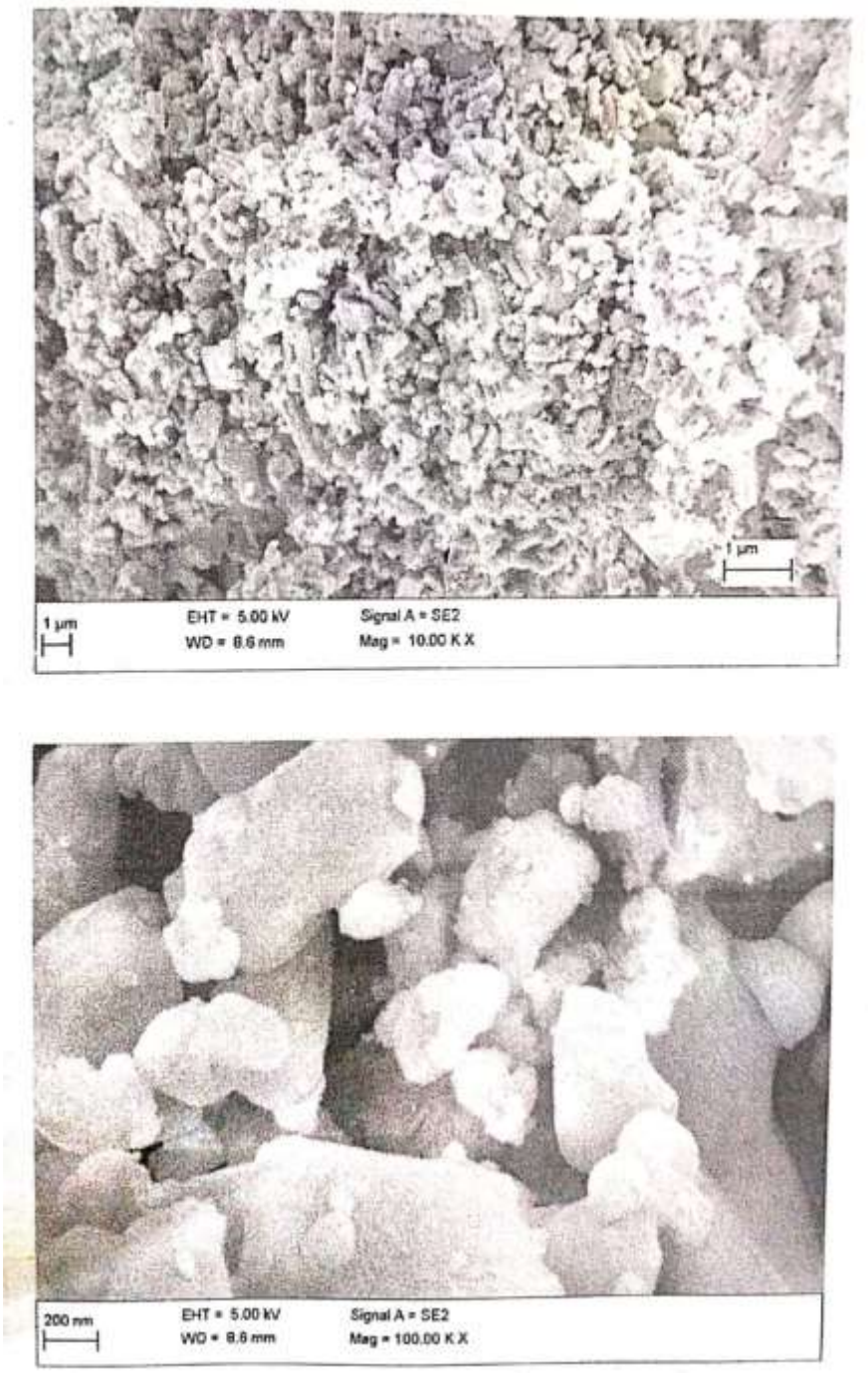

Figure 8. FESEM Images (low and high magnification) of CZTSe nanoparticles

The morphology of the CZTSe sample was observed in field emission scanning electron microscopy (FESEM) using ZEISS scanning electron micrometer Figure 3.3 shows the morphology of the as prepared CZTSe nanoparticles which reveals that the powder contains several spherical shaped ranoparticles of diameter -20mn. This nature was randomly distributed in the powder sample

5.4 COMPOSITIONAL ANALYSIS BY EDS

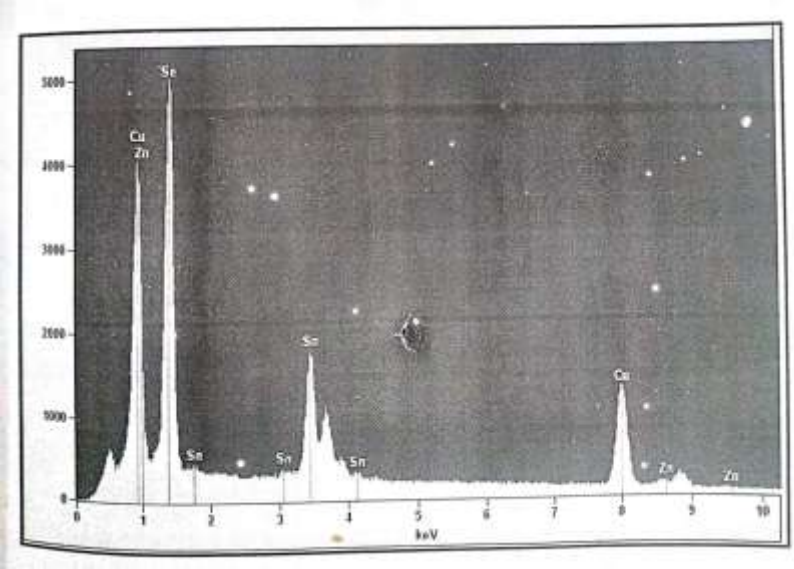

Figure 9. EDS spectrum of CZTSe nanoparticles

From EDS investigation of CZTSe nanoparticles, it is understood that they are formed with the perfect stoichiometric ratio of the already existed CZTSe stoichiometric ratio that 2:11.4. Further it suggests that the elemental ratio of Cu/Zn and Cu/Zn+(Sn+Se) is quite higher when compared with literatures . This strongly confirms that the prepared CZTSe nanoparticles are stoichiometrically controlled with their constituent elements.

5.5 ELEMENTAL MAPPING OF CZTSe

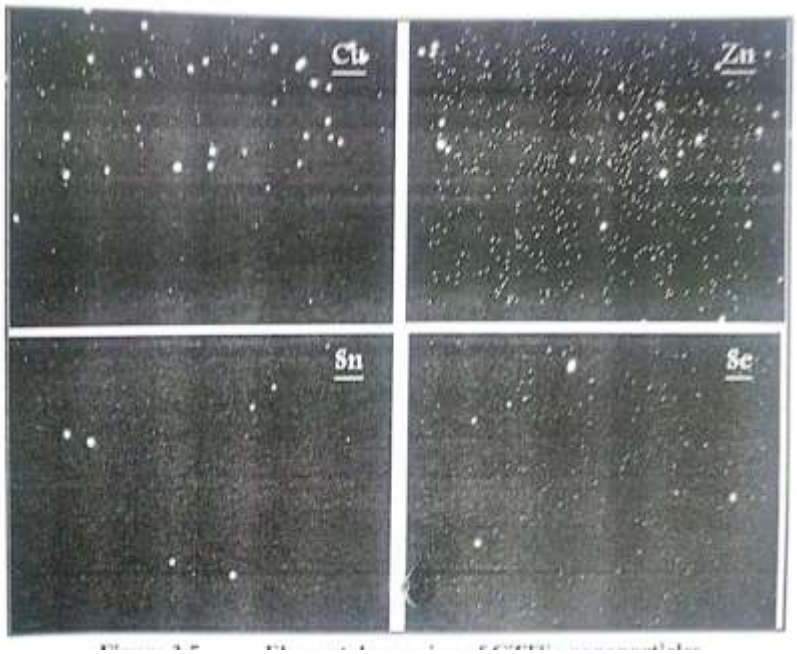

Figure 10. Elemental mapping of CZTSe nanoparticles

Atomic-scale elemental imaging provides powerful insights into materials structures in real space. This technique has been recently demonstrated using aberration-corrected scanning electron microscopy (SEM) By scanning an angstrom-sized electron probe across a thin crystallme sample, oriented along a low-index zone axis, atomic-scale elemental maps are obtained by collecting either electron energy loss spectra (EELS, thus SEM-EELS)-or energy-dispersive X-ray spectra (EDS, thus SEM-EDS) The obtained EDS mapping spectra of the CZTSe nanoparticle shows the existence of stoichiometric ratio and their equal distribution in the prepared nanoparticle systems [70-76]. It also strongly confirms the formation of CZTSe in well stoichiometrically controlled manner. Also, it is understood from the EDS mapping image that all the constitute elements were stoichiometrically distributed with respect to the compositions of CZTSe nanoparticles

5.6 TEM ANALYSIS OF CZTSE NANOPARTICLES

In order to further scrutinize the crystal structure of the prepared CZTSe nanoparticles, TEM analysis was done. Low and high magnification BF-TEM image with HRTEM and SAED patterns of pentanary nanoparticles are given in figure 3.6. As evidenced by the TEM image in figure the CZTS particles were formed as nanorods of 100 mm length along with come nanometer-sized particles surrounding it. Similarly, the TEM image of CZTSe nanoparticles show agglomerated nanoparticle clusters. The stannite crystalline phase was achieved through high-resolution TEM image [77,78]. The interplanar spacing values were 0.321 mm for CZTSe nanoparticles. The d-spacing values are confirming the crystal growth orientation plames of CZTSe nanoparticles. The circular electron diffraction patterns of CZTSe nanoparticles are given in figure. It confirmed the existence of tetragonal stennite crystal structure in the synthesized compounds. The attained electron diffraction patterns were perfectly matching with the powder diffraction patterns

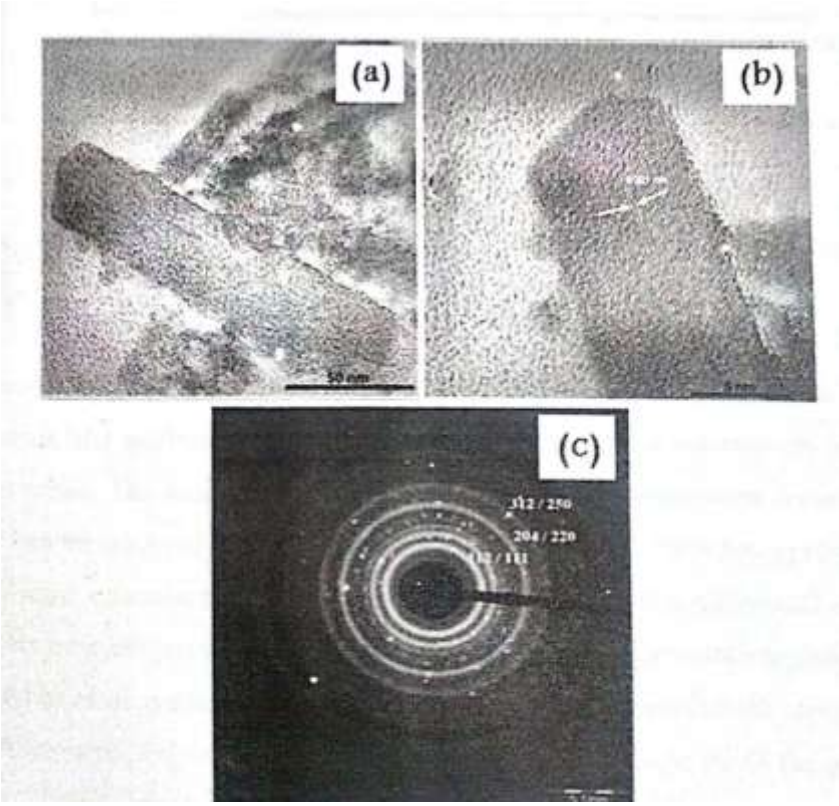

Figure 11. TEM images of CZTSe nanoparticles, (a) low magnification, (b)-high resolution TEM and (c) - SAED pattern

5.7 UV-Vis SPECTROSCOPY (UV-Vis)

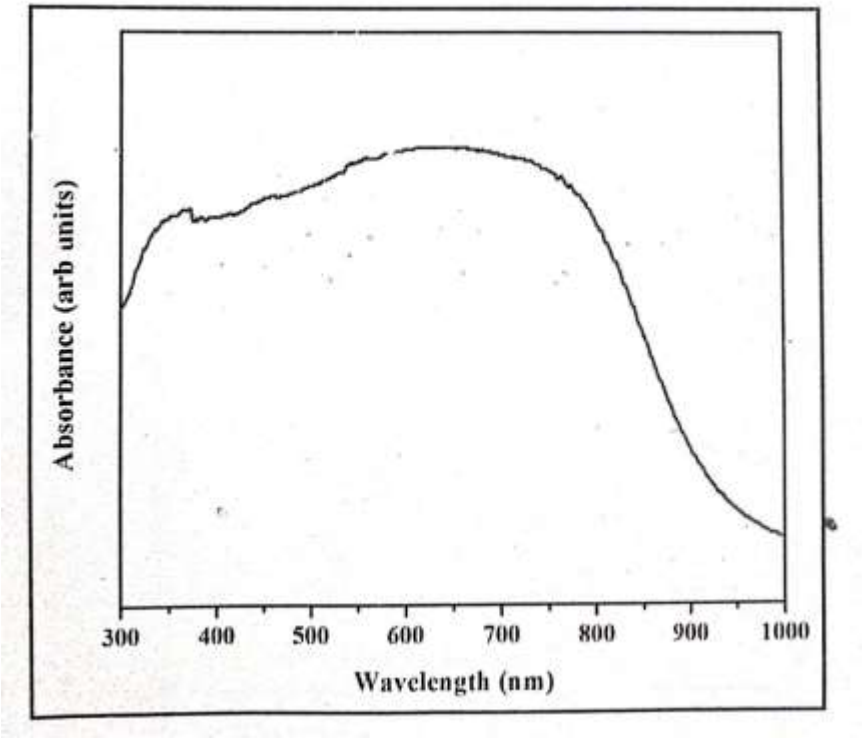

Figure 12. UV-Vis absorbance spectrum of CZTSe nanoparticles

UV-vis spectroscopy is a very useful technique which allows estimation of CZTSe concentration, and aggregation level. Moreover, UV-vis spectrometers are present in most laboratories, the analysis does not alter the sample, and the registration of the spectrum requires short times. The extinction spectra of CZTSe nanoparticles were recorded by UV-vis spectroscopy can be analysed using the Mic theory, once provided the appropriate correction of the metal dielectric constant for the nanoparticle size and the physicochemical environment, as shown by direct measurements on single nanoparticles and nanoparticles ensembles. The optical absorption studies of as synthesized CZTSe nanoparticles in the wavelength range 300-1200 nm have been investigated. Figure 3.7 shows the optical absorbance spectra of the prepared CZTSe nanoparticles. These spectra revealed that as prepared CZTSe nanoparticles have high absorbance of light in the visible region, indicating applicability as an absorbing material. The absorption coefficient is larger than 10 cm' in the visible region, which is consistent with those reported in earlier results, and therefore, the particle is considered to be a suitable material for photovoltaic solar energy conversion.

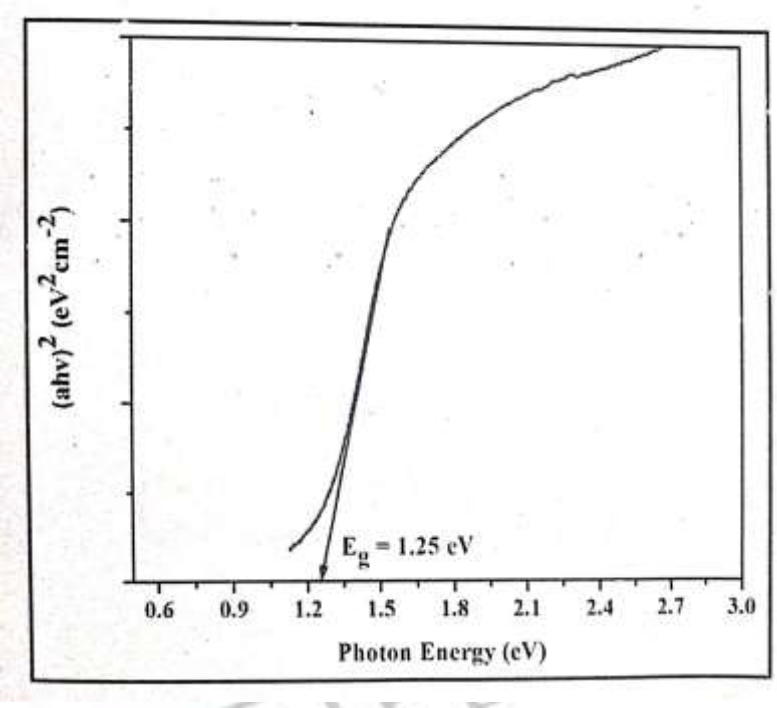

Figure 13. Band gap determination using Tauc's plot method for CZTSe nanoparticles

The optical band gap energy is estimated using the following equation for a semiconductor:

$$(\alpha h\nu) = A(h\nu - E_g)^n$$

where α is the absorption coefficient, $E_g$is the band gap energy, A is a constant, and $n = 1/2$for a direct allowed transition. Figure 12 shows the variation of $(\alpha h\nu)^2$versus $h\nu$, which exhibits a straight-line behavior in the higher energy region, indicating a direct optical transition. Extrapolation of the linear portion of the curve to zero absorption coefficient ($\alpha = 0$) gives a band gap energy of 1.255 eV for the prepared CZTSe nanoparticles. This value is in good agreement with the band gaps reported for CZTSe films by other authors. The band gap of the CZTSe nanoparticles is close to the optimum band gap required for solar cell applications, indicating that CZTSe is a promising material for thin-film solar cells. From this study, the following fruitful results have been proposed.

VI. SUMMARY AND CONCLUSION

- CZTSe chalcogenide p-type semiconducting nanoparticles were successfully synthesized using the hydrothermal method in a basic aqueous medium. The prepared nanoparticles exhibited particle sizes in the range of 15–20 nm.
- The synthesized CZTSe nanoparticles showed a band gap energy of approximately 1.25 eV, which is comparable with the standard reported value. The CZTSe nanoparticle sample prepared via non-surfactant (non-capping agent) mediated growth exhibited good crystallinity and a pure single-phase CZTSe with a kesterite tetragonal crystal structure.
- However, the exact role of the surfactant could not be clearly visualized from the SEM images due to the resolution limitation of SEM in the micrometer range. Further analysis of the surfactant effect and particle morphology requires characterization using TEM.

- XRD pattern analysis confirmed the formation of a pure tetragonal kesterite crystal phase of CZTSe. The crystallite sizes calculated using the Debye–Scherrer formula were found to be in the range of 15–18 nm.
- FESEM analysis revealed spherical morphology of the CZTSe nanoparticles, and their elemental composition was confirmed through EDS measurements. Elemental mapping demonstrated a uniform distribution of all constituent elements in the prepared CZTSe compound within the expected stoichiometric range.
- TEM images showed excellent morphological features of CZTSe nanoparticles with rod-like shapes.
- UV–Vis spectroscopy revealed strong absorption capability of the prepared CZTSe nanoparticles, with absorption extending into the near-infrared region, which strongly confirms the influence of quantum confinement.
- The optical band gap of the prepared CZTSe nanoparticles was calculated using the traditional Tauc plot method and was found to be approximately 1.25 eV.
- The obtained results suggest that the prepared CZTSe nanoparticles may be suitable as an alternative absorber material for thin-film solar cell applications.

REFERENCES

1. Abdullaeva, Z. (2017). *Nanomaterials in Medicine*. In Nanomaterials in Daily Life (pp. 67–89). Springer.
2. Acton, Q. A. (2013). *Solar Cells: Advances in Research and Application*. Scholarly Editions, Atlanta, GA.
3. Adelifard, M. (2016). Preparation and characterization of Cu_2FeSnS_4 quaternary semiconductor thin films via the spray pyrolysis technique for photovoltaic applications. *Journal of Analytical and Applied Pyrolysis*, 122, 209–215.
4. Ahmed, S., Reuter, K. B., Gunawan, O., Guo, L., Romankiw, L. T., & Deligianni, H. (2012). A high-efficiency electrodeposited Cu_2ZnSnS_4 solar cell. *Advanced Energy Materials*, 2(2), 253–259.
5. Aljammouri, T., Aazou, S., Mahboub, O., Laghfour, Z., Bouzbib, M., Abd-Lefdil, M., Ulyashin, A., Slaoui, A., & Sekkat, Z. (2016). Kesterite/wurtzite Cu_2ZnSnS_4 nanocrystals: Synthesis and characterization for PV applications. In *Proceedings of the 2016 International Renewable and Sustainable Energy Conference (IRSEC)*. IEEE.
6. Alwin, S., Menon, R., Nabhiraj, P., & Ananthapadmanabhan, P. (2017). Plasma-treated TiO_2 aerogel nanostructures as photoanode material and its influence on the performance of quasi-solid dye-sensitized solar cells. *Materials Research Bulletin*, 86, 201–208.
7. Alwin, S., Shajan, X. S., Karuppasamy, K., & Warrier, K. G. K. (2017). Microwave-assisted synthesis of high surface area TiO_2 aerogels: A competent photoanode material for quasi-solid dye-sensitized solar cells. *Materials Chemistry and Physics*, 196, 37–44.
8. Andersson, B. A. (2000). Materials availability for large-scale thin-film photovoltaics. *Progress in Photovoltaics: Research and Applications*, 8(1), 61–76.
9. Aono, M., Yoshitake, K., & Miyazaki, H. (2013). XPS depth profile study of CZTSe thin films prepared by spray pyrolysis. *Physica Status Solidi (c)*, 10(7–8), 1058–1061.
10. Araki, H., Kubo, Y., Jimbo, K., Maw, W. S., Katagiri, H., Yamazaki, M., Oishi, K., & Takeuchi, A. (2009). Preparation of Cu_2ZnSnS_4 thin films by sulfurization of co-electroplated Cu–Zn–Sn precursors. *Physica Status Solidi (c)*, **6**(5), 1266–1268.
11. Arba, Y., Rafi, M., Hartiti, B., Ridah, A., & Thevenin, P. (2011). Preparation and properties of CZTSe thin films prepared by spray pyrolysis. *Moroccan Journal of Condensed Matter*, **13**(3).
12. Arici, E., Meissner, D., Schäffler, F., & Sariciftci, N. S. (2003). Core/shell nanomaterials in photovoltaics. *International Journal of Photoenergy*, **5**(4), 199–208.
13. Aydil, E. S. (2007). Nanomaterials for solar cells. *Nanotechnology*, **4**, 275.

14. Babu, G. S. D., Shajan, X. S., George, A., Parameswaran, P., Murugesan, S., Divakar, R., Mohandas, E., Kumaresan, S., & Rao, G. M. (2017). Low-cost hydrothermal synthesis and characterization of pentanary $Cu_2ZnNiSnS_4$ nanoparticle inks for thin-film solar cell applications. *Materials Science in Semiconductor Processing*, **63**, 127–136.
15. Bhushan, B., Luo, D., Schricker, S. R., Sigmund, W., & Zauscher, S. (2014). *Handbook of Nanomaterials Properties*. Springer Science & Business Media.
16. Bitri, N., Dridi, S., Chaabouni, F., & Abaab, M. (2017). Studies on the electrical properties of Cu_2NiSnS_4 thin films prepared by a simple chemical method. *Materials Letters*.
17. Bonamico, M., Dessy, G., Mugnoli, A., Vaciago, A., & Zambonelli, L. (1965). Structural studies of metal dithiocarbamates II: The crystal and molecular structure of copper diethyldithiocarbamate. *Acta Crystallographica*, **19**(6), 886–897.
18. Bosson, C., Birch, M., Halliday, D., Knight, K., Gibbs, A., & Hatton, P. (2017). Cation disorder and phase transitions in the structurally complex solar cell material Cu_2ZnSnS_4. *Journal of Materials Chemistry A*, **5**(32), 16672–16680.
19. Brew, K. W. (2015). Processing of thin-film photovoltaics from chalcogenide nanoparticles.
20. Bucherl, C. N., Oleson, K. R., & Hillhouse, H. W. (2013). Thin-film solar cells from sintered nanocrystals. *Current Opinion in Chemical Engineering*, **2**(2), 168–177.
21. Casa, X. (2010). *CASA XPS: Processing Software for XPS, AES, and SIMS, Version 2.3.16*. Casa Software Ltd., Teignmouth, UK.

JAAFR INTERNATIONAL RESEARCH JOURNAL
JOURNAL OF ADVANCE AND FUTURE RESEARCH
JAAFR.ORG | ISSN : 2984-889X
An International Open Access, Peer-reviewed, Refereed Journal

REACTIVE YELLOW 14 DYE BY USING IXORA COCCINEA

Dhivya R
Head, Assistant Professor
Department of Chemistry
Sri Sarada Niketan College of Science for Women, Karur, India.

Abstract

The present study investigates the potential of *Ixora coccinea* leaf powder (ICLP) as a natural biosorbent for the removal of Reactive Yellow-14 (RY-14) dye from aqueous solutions. The leaves were collected, cleaned, dried, powdered, and characterized using Infrared (IR) spectroscopy and Scanning Electron Microscopy (SEM) to evaluate their surface morphology and functional groups. Batch adsorption experiments were conducted to study the effects of biomass dose, contact time, pH, and initial dye concentration on dye removal. Kinetic studies were performed using pseudo-first-order and pseudo-second-order models, while adsorption isotherms were analyzed using Langmuir, Freundlich, and Temkin models. The results revealed that maximum dye removal (72.38%) occurred at pH 2, with an optimal biomass dose of 1.9 g and an equilibrium time of 240 minutes. Adsorption data best fitted the Freundlich model, indicating multilayer adsorption on a heterogeneous surface, and kinetic analysis suggested pseudo-first-order behavior. The study demonstrates that ICLP is an effective, eco-friendly, and low-cost biosorbent for treating dye-contaminated water, providing an alternative to conventional chemical methods.

Key words

Ixora coccinea, Reactive Yellow-14 dye, Biosorption, Adsorption kinetics, Freundlich isotherm, Eco-friendly dye removal

I. INTRODUCTION

Water contamination due to synthetic dyes is a major environmental concern, as these dyes are toxic, non-biodegradable, and can cause serious health and ecological issues. Among various treatment methods, adsorption is recognized as one of the most efficient techniques due to its simplicity, cost-effectiveness, and high removal efficiency. Natural plant-based adsorbents have gained attention in recent years for wastewater treatment because they are renewable, biodegradable, and environmentally friendly.

Ixora coccinea, commonly known as jungle geranium or flame of the woods, is a flowering shrub belonging to the Rubiaceae family. Traditionally, it has been used in Ayurveda and folk medicine for its therapeutic properties, and its leaves, flowers, and roots contain bioactive phytochemicals such as lupeol, ursolic acid, oleanolic acid, sitosterol, rutin, anthocyanins, and proanthocyanidins. These functional compounds provide active sites for adsorption, making *Ixora coccinea* a promising biosorbent for dye removal.

This study aims to explore the potential of *Ixora coccinea* leaf powder (ICLP) as a natural biosorbent for the removal of Reactive Yellow-14 dye from aqueous solutions, with a focus on understanding the influence of process parameters, adsorption kinetics, and equilibrium behavior.

II. AIM AND OBJECTIVE OF THE STUDY

The aim of the project is to investigate the effectiveness of *Ixora coccinea* leaves as a natural, low-cost, and eco-friendly adsorbent for the removal of Reactive Yellow 14 dye from aqueous solutions. The objectives of this study include preparing the *Ixora coccinea* leaf adsorbent and evaluating its dye removal efficiency, studying the effect of initial dye concentration, contact time, and pH on the adsorption process, and analyzing adsorption kinetics to understand the rate and mechanism of adsorption. In addition, adsorption isotherm models are examined to describe the adsorption behavior, and desorption studies are carried out to assess the reusability of the adsorbent and the feasibility of its application in wastewater treatment.

III. DYES

A dye is a colored substance that has an affinity for the substrate to which it is applied. Dyes are generally applied in aqueous solutions and may require a mordant to improve fixation on the fiber. Both dyes and pigments are colored substances because they absorb certain wavelengths of visible light. However, dyes are usually soluble in water, whereas pigments are insoluble. Some dyes can be rendered insoluble by the addition of salts to produce lake pigments.

Dyes can be broadly classified into natural, synthetic, and organic dyes. In the present study, synthetic dyes are used. Synthetic dyes are primarily derived from petroleum sources, sometimes in combination with mineral-based components. The first synthetic organic dye, mauveine, was discovered accidentally by William Henry Perkin in 1856. Since then, a wide variety of synthetic dyes have been developed and used extensively in different industries.

3.1 Types of Dyes

Dyes are classified based on their solubility, chemical nature, and method of application.

3.1.1 Natural Dyes

Natural dyes are mainly derived from plant sources such as roots, berries, bark, leaves, and wood. Throughout history, people have dyed textiles using locally available natural materials. Rare dye sources that produced bright and permanent colors, such as Tyrian purple and crimson kermes, were highly valued in ancient and medieval times. Plant-based dyes such as indigo, woad, saffron, and madder were commercially cultivated and traded widely in Asia and Africa.

Archaeological evidence indicates that dyed flax fibers were found in a prehistoric cave in the Republic of Georgia, dating back to approximately 36,000 BP. In India, dyeing has been practiced for over 5,000 years using dyes derived from plants, animals, and minerals with minimal processing. Despite their historical importance, the large-scale use of natural dyes declined after the discovery of synthetic dyes in the late 19th century.

3.1.2 Synthetic Dyes

Synthetic dyes are man-made dyes produced mainly from petroleum-based raw materials. The discovery of mauveine by William Henry Perkin marked the beginning of the synthetic dye industry. This discovery was followed by the development of many other dyes such as fuchsine, safranine, and induline. Today, thousands of synthetic dyes are available, offering a wide range of colors, improved fastness, and cost-effectiveness.

3.1.3 Organic Dyes

Most dyes are organic compounds that may be either natural or synthetic. In addition to textile coloration, organic dyes are used in various applications such as dye lasers, optical recording media, and camera sensors. This classification is based on the chemical structure of the dye molecules.

3.2 Classification Based on Application

Acid Dyes

Acid dyes are water-soluble anionic dyes applied to fibers such as silk, wool, nylon, and modified acrylic fibers under acidic conditions. The dye-fiber interaction occurs mainly through ionic bonding. Most synthetic food colors belong to this category. **Examples: Acid Red 88, Alizarin Pure Blue B.**

Basic Dyes

Basic dyes are water-soluble cationic dyes primarily used for acrylic fibers, with limited application on wool and silk. Acetic acid is often added to the dye bath to enhance dye uptake. Basic dyes are also used in paper coloration.

Direct (Substantive) Dyes

Direct dyes are applied in neutral or slightly alkaline dye baths, usually at or near boiling temperature, with the addition of sodium chloride or sodium sulfate. These dyes are used for cotton, paper, leather, wool, nylon, and silk. They are also used as pH indicators and biological stains.

Mordant Dyes

Mordant dyes require the use of a mordant to improve dye fastness against washing, light, and perspiration. Different mordants can significantly alter the final color of the dye. Many natural dyes fall under this category. Synthetic mordant dyes, also known as chrome dyes, are mainly used for wool. It should be noted that some mordants, especially heavy metal salts, may be hazardous to health.

Vat Dyes

Vat dyes are water-insoluble dyes that cannot dye fibers directly. They are reduced in an alkaline medium to form a water-soluble leuco compound, which has an affinity for textile fibers. After dyeing, oxidation converts the dye back to its insoluble form within the fiber.

Reactive Dyes

Reactive dyes contain a chromophore with a reactive group that forms a covalent bond with the fiber. This strong bond makes reactive dyes highly colorfast. They are widely used for dyeing cotton and other cellulose fibers and can be applied at room temperature in the case of cold reactive dyes.

Disperse Dyes

Disperse dyes are water-insoluble dyes developed primarily for synthetic fibers such as polyester. They are finely ground and applied using dispersing agents. High dyeing temperatures or pressurized dye baths are often required. These dyes can also be used for nylon, cellulose triacetate, and acrylic fibers.

Azoic Dyes

Azoic dyes are produced directly on the fiber by the reaction of diazo and coupling components under controlled dye bath conditions. This method is mainly used for cotton. However, the use of azoic dyes has declined due to the toxic nature of the chemicals involved.

Sulfur Dyes

Sulfur dyes are inexpensive dyes used mainly for dyeing cotton in dark shades. Dyeing is carried out by heating the fabric in a solution containing sulfur compounds, resulting in dark colors with good wash fastness.

IV. IXORA COCCINEA

The name *Ixora* is derived from the Sanskrit word *Ikvana*, associated with Iswara, a Malaysian deity to whom flowers were traditionally offered. The species name *coccinea* means scarlet, referring to the bright red color of the flowers. *Ixora coccinea*, commonly known as jungle geranium, flame of the woods, or jungle flame, is a species of flowering plant belonging to the family Rubiaceae. It is a popular ornamental shrub native to Southern India, Bangladesh, and Sri Lanka. Due to its attractive appearance and adaptability, *Ixora coccinea* is widely cultivated in tropical and subtropical regions and has become a common landscape plant in South Florida. It is also recognized as the national flower of Suriname.

Figure.1 Ixora Coccinea

Taxonomical Classification

- **Kingdom:** Plantae
- **Order:** Gentianales
- **Family:** Rubiaceae
- **Subfamily:** Ixoroideae
- **Tribe:** Ixoreae
- **Genus:** *Ixora*
- **Species:** *Ixora coccinea*

Cultivation and Uses

Although the genus *Ixora* comprises nearly 500 species, only a few are commonly cultivated, with *Ixora coccinea* being the most widely grown. It is extensively used in warm climates for hedges, screens, foundation plantings, and mass flowering beds, and may also be grown as a specimen shrub or small tree. In cooler climates, it is cultivated in greenhouses or as a potted indoor plant requiring bright light. The plant is also suitable for container gardening and is often used as a decorative patio or poolside plant.

Ixora coccinea is a compact, densely branched shrub that tolerates pruning well, making it ideal for formal hedges, although it exhibits optimal growth when not heavily sheared. Numerous cultivars are available, varying in flower color such as yellow, pink, and orange, as well as in plant size. Popular dwarf cultivars include ‘Nora Grant’, while ‘Super King’ is known for its large flower clusters. The development of new cultivars and hybrids in recent decades has led to renewed interest in this ornamental plant.

Medicinal and Chemical Properties

Various parts of *Ixora coccinea*, including flowers, leaves, roots, and stems, are used in traditional Indian medicine (Ayurveda) and in folk medicinal practices for the treatment of different ailments. The ripe fruits are also consumed as a dietary source.

Phytochemical studies have revealed that *Ixora coccinea* contains several bioactive compounds such as lupeol, ursolic acid, oleanolic acid, sitosterol, rutin, leucocyanidin, anthocyanins, proanthocyanidins, and glycosides of kaempferol and quercetin. The flowers yield an attractive pinkish-red pigment due to the presence of anthocyanins. Extracts of *Ixora coccinea* have been utilized for color fixation and have also been used in the formulation of herbal products such as lip balms, reported to have no adverse side effects.

V. EXPERIMENTAL METHODS

5.1 Preparation of Biomass

Fresh leaves of *Ixora coccinea* were collected from Mottankurichi. The collected leaves were thoroughly washed with tap water to remove soil and dust particles, followed by washing with distilled water. The cleaned leaves were dried, powdered, and sieved to obtain a particle size of 4.25 µm. The powdered biomass was again washed with distilled water and dried under sunlight until all moisture was completely removed. The dried biomass was stored in airtight glass bottles for further use.

5.2 Preparation of Stock Solution

A stock solution of Reactive Yellow dye with a concentration of 1000 ppm was prepared by dissolving 1 g of Reactive Yellow dye in distilled water and making up the volume to 1000 mL. Distilled water was used for the preparation of all solutions. All adsorption experiments were conducted at room temperature.

5.3 Effect of Biomass Dose on Reactive Yellow Dye Adsorption

To determine the minimum amount of biomass required for maximum dye removal, a series of 100 mg/L dye solutions were taken in stoppered reagent bottles. Different quantities of *Ixora coccinea* leaf biomass ranging from 0.1 g to 1.9 g were added to the bottles. The mixtures were agitated using a mechanical shaker for three hours to attain equilibrium. After equilibration, the solutions were allowed to settle, and the absorbance of the supernatant was measured using a UV–Visible spectrophotometer. The percentage of dye removal was calculated based on the absorbance values obtained.

5.4 Effect of Contact Time

To study the effect of contact time, 100 mL of dye solution was taken in ten reagent bottles. To each bottle, 1 g of powdered *Ixora coccinea* biomass was added. The bottles were agitated in a mechanical shaker. Samples were withdrawn at different time intervals of 10 minutes (for the first three bottles) and 30 minutes (for the remaining bottles). After withdrawal, the solutions were allowed to settle for 30 minutes, filtered, and the filtrates were analyzed using a UV–Visible spectrophotometer. The relationship between absorbance and contact time was evaluated.

5.5 Effect of pH

To investigate the effect of pH on dye adsorption, 100 mL of Reactive Yellow dye solution was taken in ten reagent bottles. The pH of the solutions was adjusted in the range of 2 to 10 using appropriate acidic or alkaline solutions. After pH adjustment, 1 g of biomass was added to each bottle, and the mixtures were shaken for one hour. The solutions were then filtered, and the absorbance of the supernatant was measured using a UV–Visible spectrophotometer.

5.6 Kinetic Studies

Adsorption kinetic studies were conducted to understand the rate and mechanism of dye adsorption. Dye solutions with concentrations of 30 ppm, 40 ppm, 50 ppm, and 60 ppm were prepared. For each concentration, six reagent bottles were taken, and 1 g of biomass was added to each bottle along with 100 mL of dye solution. The bottles were agitated in a mechanical shaker. Samples were withdrawn at time intervals of 10, 20, 30, 60, 90, and 120 minutes. The withdrawn solutions were filtered, and the absorbance was measured using a UV–Visible spectrophotometer. The same procedure was repeated for all dye concentrations. The kinetic data obtained were analyzed using appropriate adsorption kinetic models, including the Langmuir–Hinshelwood equation.

5.7 Instrumentation

The experimental work involved several instruments for accurate measurements and analysis. The powdered biomass was prepared using a mechanical grinder and sieved with a standard sieve of 4.25 µm. Analytical balances were used to weigh the biomass and dye accurately. Solutions were prepared in volumetric flasks and measured using pipettes and measuring cylinders. A mechanical shaker was used to ensure proper mixing and equilibration of the dye with the biomass. The pH of solutions was measured and adjusted using a digital pH meter. Finally, a UV–Visible spectrophotometer was employed to determine the dye concentration in the supernatant and to calculate the percentage of dye removal and adsorption kinetics.

VI. RESULTS AND DISCUSSION

6.1 Infra-Red Spectrum

Graph 1 shows the infrared (IR) spectrum of *Ixora coccinea* leaf powder. The spectrum indicates the presence of functional groups responsible for adsorption. Peaks observed at different wavenumbers suggest the availability of hydroxyl, carboxyl, and other active groups which can bind with the dye molecules.

6.2 Scanning Electron Microscopy (SEM)

The SEM micrograph of Ixora coccinea leaf powder (ICLP) before dye adsorption. The micrograph reveals that ICLP possesses a rough surface morphology with pores of various sizes. The heterogeneous surface with cavities provides suitable binding sites for adsorption of Reactive Yellow-14 dye.

6.3 Effect of Sorbent Dose

The effect of sorbent dose on the removal of RY-14 dye is shown in Table 1. As the biomass dose increased from 0.1 g to 1.9 g, the percentage of dye adsorbed increased from 21.67% to 78.07%. Maximum adsorption was achieved at 1.9 g of biomass. Therefore, this dose was used in all subsequent experiments.

S.No	Biomass Dose (g)	% of Dye Removal
1	0.1	21.67
2	0.3	23.24
3	0.5	26.87
4	0.7	33.97
5	0.9	44.27
6	1.1	54.93
7	1.3	62.88
8	1.5	70.46
9	1.7	75.01
10	1.9	78.07

Table 1: Effect of Biomass Dose on RY-14 Dye Removal

6.4 Effect of Contact Time

The effect of contact time on dye removal was studied in the range of 10–240 minutes with an adsorbent dose of 1 g/100 mL for an initial dye concentration of 100 mg/L. Table 2 summarizes the results. Maximum removal of 72.38% was achieved at 240 minutes, after which the adsorption reached equilibrium.

S.No	Time (min)	% of Dye Removal
1	10	28.68
2	20	30.79
3	30	33.63
4	60	40.34
5	90	45.36
6	120	50.01
7	150	55.61
8	180	62.08
9	210	67.20
10	240	72.38

Table 2: Effect of Contact Time on Dye Removal

6.5 Effect of pH

The effect of initial pH on dye adsorption was studied in the pH range of 2–10. Table 3 shows that maximum dye removal (81.08%) occurred at pH 2. The high adsorption at acidic pH is due to electrostatic attraction between the positively charged surface of the biomass and the negatively charged dye molecules. As the pH increased, adsorption decreased due to electrostatic repulsion.

S.No	pH	% of Dye Removal
1	2	81.08
2	3	72.38
3	4	68.72
4	5	67.31
5	6	64.00
6	7	49.91

S.No	pH	% of Dye Removal
7	8	47.12
8	9	44.07
9	10	33.83

Table 3: Effect of pH on Dye Removal

6.6 Adsorption Isotherms

Adsorption isotherms were studied by varying biomass dosage (0.1–1.9 g/L) for 100 mg/L dye solution. The amount of dye adsorbed was calculated spectrophotometrically at 375 nm.

6.6.1 Langmuir Isotherm

Langmuir isotherm assumes monolayer adsorption and is expressed as:

$$\frac{X}{m} = \frac{a \cdot b \cdot C_e}{1 + b \cdot C_e}$$

Where:

- X= Amount of dye adsorbed at equilibrium
- m= Mass of adsorbent
- C_e= Equilibrium dye concentration
- a, b= Langmuir constants

The equilibrium data correlated with Langmuir isotherm. A linear plot of C_e vs X/m gave a correlation coefficient $R^2 = 0.7857$.

5.6.2 Freundlich Isotherm

Freundlich isotherm is expressed as:

$$\log\frac{X}{m} = \log K + \frac{1}{n}\log C_e$$

Where:

- X= Amount of dye adsorbed (mg)
- m= Mass of adsorbent (mg)
- C_e= Equilibrium dye concentration
- $K, 1/n$= Freundlich constants

The linear plot of $\log(X/m)$ vs $\log C_e$ indicates good correlation, with $R^2 > 0.8771$, showing that Freundlich isotherm fits the data better than Langmuir or Temkin models.

6.7 Kinetics of Adsorption

Kinetics studies were carried out with dye concentrations of 30, 40, 50, and 60 ppm using 1 g biomass. Samples were withdrawn at intervals of 20–120 minutes, filtered, and analyzed spectrophotometrically. Adsorption was rapid, with maximum adsorption achieved within 2 hours.

Rate Constant Studies

The first-order kinetic model was applied:

$$\ln(1 - \alpha t) = -kt$$

Where:

- C_{A0}= Initial dye concentration
- C_{At}= Dye concentration at time t
- C_{Ae}= Equilibrium dye concentration

A plot of $\log(1 - \alpha)$vs contact time was linear, confirming that adsorption follows first-order kinetics. The rate constant $k_1$was calculated from the slope of the line.

VII. CONCLUSION

This study demonstrated that *Ixora coccinea* leaf powder (ICLP) can effectively remove Reactive Yellow-14 (RY-14) dye from aqueous solutions. The adsorption process was found to be highly dependent on pH, with the optimal dye removal observed at pH 2. As the sorbent dose increased, the percentage of dye removal also increased, indicating the availability of more active sites for adsorption. The adsorption equilibrium was reached at approximately 4 hours. Thermodynamic data fitted well with the Freundlich adsorption model, suggesting multilayer adsorption on heterogeneous surfaces. Kinetic studies indicated that the adsorption followed pseudo-first-order rate kinetics. Overall, this study confirms that ICLP is a promising, eco-friendly, and cost-effective biosorbent for removing Reactive Yellow-14 dye from aqueous solutions.

REFERENCES

1. Bhattacharya, "Review article: Application of natural dyes on textiles," *Indian J. Fabric and Textile Research*, 34, pp. 384–399, 1999.
2. R. Bhuyan and C. N. Saikia, "Isolation of colour components from native dye-yielding plants in Northeastern India," *Biores. Technol.*, 96(3), pp. 63–72, 2005.
3. B. Ghorpade, M. Darvekar, and P.S. Vankar, "Eco-friendly cotton dyeing with Sappan wood dye using ultrasound energy," *Colourage*, pp. 27–30, 2000.
4. D. Jothi, "Extraction of Natural Dyes from African Marigold Flowers (Tagetes erecta) for Textile Coloration," *Autex Research Journal*, 8(2), pp. 49–53, 2008.
5. BMM Kamci, II. Helmy, and N.S. Hawary, "Some studies on dyeing properties of fabrics with *Crocus sativus* (Saffron) flowers using an ultrasonic method," *Autres Research Journal*, 9(1), 2009.
6. Ado, A., Yahaya, H., Kwali, A. A., and Abdulkaita, R., "Dyeing of textiles with eco-friendly natural dyes: A review," *International Journal of Environmental Monitoring and Protection*, 1(5), pp. 76–81, 2014.
7. Aksog, B. E., and Ertan, R., "Spectral properties of chalcone II," *FABAD Journal of Pharmaceutical Science*, 37(4), pp. 205–216, 2012.
8. Aminoddin and Haji, A., "Functional dyeing of wool with natural dye extracted from *Berberis vulgaris* wood and *Rumex hymenosepolus* root as biomordant," *Iranian Journal of Chemistry and Chemical Engineering*, 3(29), pp. 55–60, 2010.
9. Arun, K.P., and Yogamoorthi, A., "Isolation, application and biochemical characterization of colour components from *Tecoma stans*: A cost-effective and eco-friendly source of natural dye," *International Journal of Natural Products Research*, 4(1), pp. 9, 2014.
10. Bhattacharya, S. D., and Shah, A. K., "Metal ion effect on dyeing of wool fabric with catechu," *Coloration Technology*, 116(1), pp. 10–12, 2000.

11. Latha L.Y., and Ibrahim, D., "Pharmacological screening of methanolic extract of *Ixora* species," *Asian Pacific Journal of Tropical Biomedicine*, 2(2), pp. 149–151, 2012.
12. Latha P.G., Abraham T.K., and Panikar K.R., "Antimicrobial properties of *Ixora coccinea* Linn," *Anc Sci Life*, 14(4), pp. 286–291, 1995.
13. Yasmeen M., and Prabhu B., "Antidiarrheal activity of flowers of *Ixora coccinea* Linn in rats," *Ayurveda Integrative Medicine*, 1(14), pp. 287–291, 2010.
14. Latha P.G., and Panikkar K.R., "Cytotoxic and antitumor principles from *Ixora coccinea* flowers," *Cancer Letters*, 130(1–2), pp. 197–202, 1998.
15. Ratsasoorya W.D., et al., "Leaves of *Ixora coccinea*," *Acta Biol Hung.*, 36(1), pp. 321–334, 2005.
16. Park J., et al., "Phytochemical activity of methanol extracts of *Ixora* flowers," *Lythracea*, 38, pp. 204–207, 2007.
17. Benkablia N., "Antimicrobial activity of various extracts of onion (*Allium cepa*) and garlic (*Allium sativum*)," *Tak*, 37, pp. 263–266, 2004.
18. *The Wealth of India: Dictionary of Indian Raw Materials and Industrial Products*, National Institute of Science Communication, New Delhi, 2000, 3, pp. 231.
19. Annapurnia, P.V.S., et al., "Antimicrobial activity of *Ixora coccinea* leaves," *Veterinary Research*, 74, pp. 291–293, 2003.
20. Yasmeen M., Prabhu B., Agashaar N.V., "Evaluation of the antidiarrhoeal activity of leaves of *Ixora coccinea* Linn in rats," *Journal of Clinical and Diagnostic Research*, 4, pp. 3298–3303, 2010.
21. Akter F., Kaisar A., et al., "Phytochemical and biological investigations of *Ixora arborsa*," *Dhaka University Journal of Pharmaceutical Sciences*, 9, pp. 161–166, 2009.
22. Alves J., and Barreto R.W., "*Paradocercospora soricola* causing leaf spots on *Ixora coccinea* in Brazil," *Plant Disease*, 94, pp. 278, 2010.
23. Ali M.A., and Kapadia Z., *Pak J. Sci. Ind. Res.*, 11, pp. 12–14, 1968.
24. Arunachalam G., Subramanian N., Pazham G.P., Kartat Ma., Ravichandran V., "Phytochemical and anti-ulcer investigations of first leaf extract of *Ixora coccinea* Linn," 2006, pp. 26–31.
25. Anjaneyalu A., et al., "Chemical investigation of some Indian plants," *Indian J. Chem.*, 3, pp. 231, 1965.
26. Saroya Anirritpalsingh, "Herbal pharmacology and phytochemistry," Enfield USA Science Publishers, 2011, pp. 2–3.
27. Patil D.A., "Origin of Plant Names," Delhi, Daya Publications, 2007, p. 151.
28. Shah G.L., *Flora of Gujarat State, Part 1*, Sardar Patel University, Vallabh Vidhyanagar, 1978, p. 353–354.
29. Khandelwal K.R., *Practical Pharmacognosy*, 19th ed., Pune: Nirali Prakashan, 2002, pp. 24–29, 149–153.
30. Elumalai A., Chinna Eawaraiah, Yetcharla V., Burle S.K., Chava N., "Phytochemical and pharmacological profile of *Ixora coccinea* Linn," *Int. J. Pharm & Life Sci.*, 3(3), pp. 1563–1567, 2012.
31. Kirtikar K.R., Basu B.D., *Indian Medicinal Plants*, Dehradun (India), Oriental Enterprises, 2001, pp. 1754–1786.
32. Kumar G.S., *Regulatory Roadmap for Herbal Medicines*, New Delhi: Business Horizons, 2007, pp. 1–2.
33. Saruya A.S., *Glossary of Phytochemicals*, New Delhi: Business Horizons, 2006, p. 223.
34. Taleb-Contini S.H., Salvador M.J., Balanço J.M.F., Albuquerque S., De Oliveira D.C.R., "Antiprotozoal effects of crude extracts and flavonoids from *Chromolaena hirsuta* (Asteraceae)," *Phytother. Res.*, 18, pp. 250–254, 2004.